Natural Resources Canada
Ressources naturelles Canada

Nueltin granites and mafic rocks in the Tebesjuak Lake map area, Nunavut: new geochronological, petrological, and geophysical data

T.D. Peterson, J.M.J. Scott, A.N. LeCheminant, V.L. Tschirhart, L.B. Chorlton, W.J. Davis, and M.A. Hamilton

Geological Survey of Canada
Current Research 2015-5

2015

Canada

Geological Survey of Canada
Current Research 2015-5

Nueltin granites and mafic rocks in the Tebesjuak Lake map area, Nunavut: new geochronological, petrological, and geophysical data

T.D. Peterson, J.M.J. Scott, A.N. LeCheminant, V.L. Tschirhart, L.B. Chorlton, W.J. Davis, and M.A. Hamilton

2015

ISSN 1701-4387
Catalogue No. M44-2015/5E-PDF
ISBN 978-1-10025839-3
doi:10.4095/296163

A copy of this publication is also available for reference in depository libraries across Canada through access to the Depository Services Program's Web site at http://dsp-psd.pwgsc.gc.ca

This publication is available for free download through GEOSCAN
http://geoscan.ess.nrcan.gc.ca

Recommended citation

Peterson, T.D, Scott, J.M.J., LeCheminant, A.N., Tschirhart, V.L., Chorlton, L.B., Davis, W.J., and Hamilton, M.A., 2015. Nueltin granites and mafic rocks in the Tebesjuak Lake map area, Nunavut: new geochronological, petrological, and geophysical data; Geological Survey of Canada, Current Research 2015-5, 19 p. doi:10.4095/296163

Critical review
B. Kjarsgaard

Authors
T.D. Peterson (Tony.Peterson@NRCan-RNCan.gc.ca)
J.M.J. Scott (justtrickin@hotmail.com)
A.N. LeCheminant (Tony.LeCheminant@NRCan-RNCan.gc.ca)
V.L. Tschirhart (Victoria.Tschirhart@NRCan-RNCan.gc.ca)
L.B. Chorlton (Lesley.Chorlton@NRCan-RNCan.gc.ca)
W.J. Davis (Bill.Davis@NRCan-RNCan.gc.ca)
Geological Survey of Canada
601 Booth Street
Ottawa, Ontario
K1A 0E8

M.A. Hamilton (mahamilton@es.utoronto.ca)
Jack Satterly Geochronology Laboratory
Department of Earth Sciences
University of Toronto
Toronto Ontario

Correction date:

Nueltin granites and mafic rocks in the Tebesjuak Lake map area, Nunavut: new geochronological, petrological, and geophysical data

T.D. Peterson, J.M.J. Scott, A.N. LeCheminant, V.L. Tschirhart, L.B. Chorlton, W.J. Davis, and M.A. Hamilton

Peterson, T.D, Scott, J.M.J., LeCheminant, A.N., Tschirhart, V.L., Chorlton, L.B., Davis, W.J., and Hamilton, M.A., 2015. Nueltin granites and mafic rocks in the Tebesjuak Lake map area, Nunavut: new geochronological, petrological, and geophysical data; Geological Survey of Canada, Current Research 2015-5, 19 p. doi:10.4095/296163

Abstract: We report new and refined legacy data on 1.77 to 1.74 Ga gabbros, basalts, and granites (Kivalliq Igneous Suite) in the Tebesjuak Lake map area (NTS 65-O). Uranium-lead (baddeleyite) ages for a coarse alkali gabbro at Mallery Lake (1769 ± 6 Ma) and for a subalkaline gabbro at the southwestern end of the McRae Lake dyke (1753.6 ± 1.2 Ma) were determined. Uranium-lead (zircon) ages of 1752.6 ± 4.1 Ma and 1746.7 ± 4.3 Ma were obtained for the Pamiutuq granite intrusion and a quartz-feldspar porphyry dyke, respectively. Gravimetric/magnetic modelling of the Mallery complex is consistent with a gabbroic ring dyke about 8 km in diameter and 1 km tall surrounding a granite core, with an underlying mafic sill or intrusive complex. Petrographic and geochemical data support a petrogenetic link between the Mallery gabbro, a coarse anorthosite body (Fish intrusion), and basaltic lavas in the map area, all of alkali basalt composition. These data indicate the presence of bimodal volcanism near the base of the Pitz Formation, and establish the oldest age of Kivalliq anorogenic igneous activity at ca. 1.77 Ga.

Résumé : Nous présentons de nouvelles données ainsi que d'anciennes données rendues plus précises sur des gabbros, basaltes et granites âgés de 1,77 à 1,74 Ga (suite magmatique de Kivalliq) dans la région cartographique de Tebesjuak Lake (SNRC 65-O). On a daté par géochronologie U-Pb (sur baddeleyite) un gabbro alcalin à grain grossier au lac Mallery (1769 ± 6 Ma) et un gabbro subalcalin à l'extrémité sud-ouest du dyke de McRae Lake (1753,6 ± 1,2 Ma). Par géochronologie U-Pb (sur zircon), on a obtenu un âge de 1752,6 ± 4,1 Ma pour l'intrusion granitique de Pamiutuq et un âge de 1746,7 ± 4,3 Ma pour un dyke de porphyre à quartz-feldspath. Les résultats de la modélisation gravimétrique/magnétique du complexe de Mallery sont compatibles avec un filon annulaire de gabbro d'un diamètre de 8 km et d'une hauteur de 1 km disposé autour d'un noyau de granite, le tout surmontant un filon-couche ou un complexe intrusif mafique. Les données pétrographiques et géochimiques étayent l'existence d'un lien pétrogénétique entre le gabbro de Mallery, un massif d'anorthosite à grain grossier (intrusion de Fish) et des laves basaltiques dans la région cartographique, des lithologies qui présentent toutes une composition de basalte alcalin. Ces données indiquent l'existence d'un volcanisme bimodal près de la base de la Formation de Pitz et établissent l'âge le plus ancien pour l'activité ignée anorogénique de la suite de Kivalliq à environ 1,77 Ga.

INTRODUCTION

Proterozoic granites in the Kivalliq region of Nunavut (Hudson Suite, ca. 1.83 Ga; Nueltin Granite, ca. 1.75 Ga: van Breemen et al., 2005) are a distinctive part of the bedrock near the Lone Gull (Kiggavik) uranium deposit, and were studied as part of the GEM-1 Uranium project, which was anchored in the Kiggavik area (Jefferson et al., 2011a,b; Scott, 2012). The younger Nueltin event imposed a metasomatic overprint on Hudson granites and Martell syenites adjacent to Kiggavik uranium mineralization (Scott et al., in press), which is an unconformity-type deposit (Fuchs and Hilger, 1989). Kiggavik is 50 km north of NTS 65-O (Tebesjuak Lake, Figure 1), where a large volume of Nueltin-age intrusions and cogenetic volcanic rocks of the Pitz Formation (upper Wharton Group) is present (Peterson et al., 2014). The Wharton Group is the central portion of the tripartite Dubawnt Supergroup (Fig. 2), which was deposited in epicontinental basins over approximately 300 million years (ca. 1.85–1.55 Ga).

This study re-evaluated specific intrusive and extrusive units in NTS 65-O as part of the Geo-Mapping for Energy and Minerals program (GEM) to address questions on the nature and timing of Nueltin-aged mafic and silicic igneous activity, and its relationship to Au-Ag and Pb-Cu mineral showings in the area. Previous field studies identified extensive Proterozoic bimodal (granite-gabbro) plutonism and basalt-rhyolite volcanism between Tulemalu Lake and Mallery Lake, within NTS 65-O (Fig. 1) (LeCheminant et al., 1979a, 1979b, 1980, 1981; LeCheminant, 1981). Mafic rocks of the Pitz-Nueltin system were also identified in the Dubawnt Lake area prior to the GEM study (Peterson, 2006), but the Tebesjuak Lake map area contains a relatively large volume of them, as well as rapakivi-textured Nueltin Granite; porphyritic, glassy, and topaz-bearing rhyolites

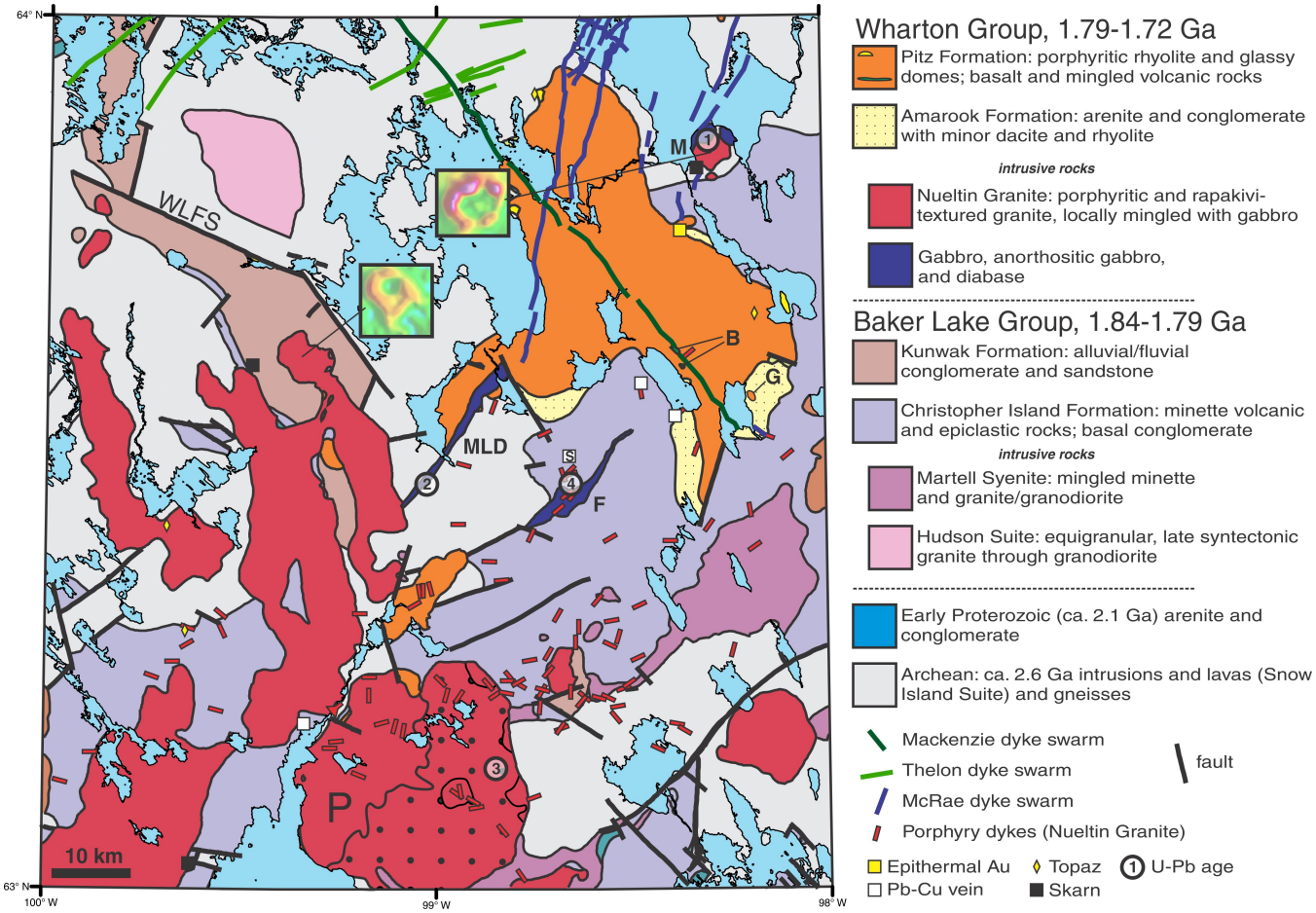

Figure 1. Geology, Tebesjuak Lake (65-O), simplified from Peterson et al. (2014). WLFS = Wharton Lake fault zone, M = Mallery complex, MLD = McRae Lake dyke, F = Fish intrusion, P = Pamiutuq intrusion, B = basalt outcrops, G = aphyric (formerly glassy) rhyolite dome. U-Pb age locations: 1 = Mallery gabbro; 2 = McRae Lake dyke; 3 = Pamiutuq intrusion; 4 = porphyry dyke. S = Spec Pb-Cu showing. Yellow subunit of Pitz Formation indicates aphyric rhyolite, sometimes topaz-bearing. The patterned area within the Pamiutuq intrusion has high magnetic susceptibility and represents a portion where mingling textures with basalt are prominent. Inset boxes show magnetic anomaly maps, to scale, indicating the presence of gabbroic ring dykes and/or magnetite-bearing skarns.

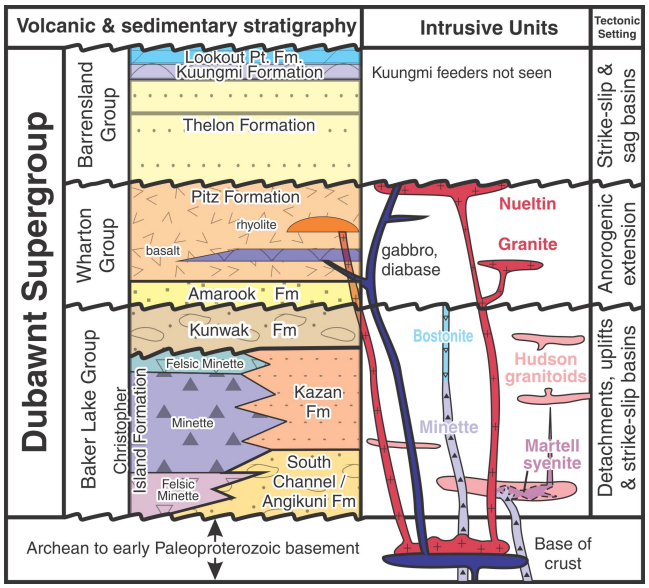

Figure 2. Stratigraphy of the Dubawnt Supergroup (*after* Peterson et al., 2015).

(Peterson et al., 2014 and references therein); epithermal chalcedony-fluorite with anomalous Au-Ag (Biczok, 1996); and a Pb-Cu showing previously linked to emplacement of Nueltin-age granites (the Spec showing: Webb, 1981).

The following units in NTS 65-O were targeted for study.

1. The Mallery complex (new term), consists in part of a mafic intrusive body with previously unknown petrological and temporal links to Nueltin plutonism, that is in contact with the Nueltin Granite, and is spatially associated with epithermal quartz-fluorite bodies;
2. A 20 km long body of coarse anorthosite, termed the Fish intrusion, is parallel to and 15 km east-southeast of the McRae Lake dyke, and is flanked by three Cu-Pb showings. The Fish intrusion is cut by quartz-feldspar porphyry dykes correlated with rapakivi-textured Nueltin-age granites, and had previously unknown relationships with other mafic rocks of the area;
3. Basaltic extrusive rocks are exposed adjacent to a Mackenzie diabase dyke north of the Fish intrusion. Petrological studies were conducted to resolve their relationship to mafic intrusions in the area;
4. The McRae Lake dyke is a gabbroic body 23 km long and up to 1.8 km wide (Tambosso, 1981), which lies at the origin of a swarm of diabase dykes (the McRae Lake dyke swarm) that extends an additional 600+ km to the northeast through Schultz Lake and beyond the Amer Fault Zone. An accurate emplacement age for the McRae Lake dyke was required for regional correlations;
5. The Pamiutuq granite (Booth, 1983) is a circular, subvolcanic intrusion on the north side of Tulemalu Lake (Fig. 1) which displays abundant mingling between granitic and mafic magmas, on centimetre to kilometre scales. Its emplacement age and that of an extensive swarm of quartz-feldspar porphyry dykes which cut the Pamiutuq and Fish intrusions needed resolution.

Whole rock elemental and isotopic analyses from this study are reported in Peterson et al. (2015) and are cited here in support of our interpretations. Our results are consistent with the Tebesjuak Lake map area coinciding with the most active portion of the 1.77 to 1.74 Ga igneous province, now termed the Kivalliq Igneous Suite (Peterson et al., 2014), with intrusive and extrusive rocks spanning and exceeding the age range of Nueltin granites previously delineated by van Breemen et al. (2005). The Nueltin Granite, formerly assigned suite status (Peterson and van Breemen, 1999), is now subsumed under the Kivalliq Igneous Suite, which comprises a classic anorogenic bimodal igneous province. Magmatism postdates all ductile deformation, and the intrusive and supracrustal rocks are affected only by brittle faults.

Figure 1, a simplified geological map of NTS 65-O *after* Peterson et al. (2014), includes the location of four new U-Pb age determinations (this study), as well as numerous mineral showings. We have reinterpreted four sediment-dominated exposures flanking the large unit of Pitz Formation that were assigned by LeCheminant (1981) to the Kunwak Formation (upper Baker Lake Group) as part of the Amarook Formation (Rainbird et al., 2003), as they contain dacite and rhyolite volcanic rocks typical of the Wharton Group.

SUMMARY DESCRIPTIONS, PETROLOGY, AND GEOPHYSICS

Mallery complex

Mallery gabbro and anorthosite

The Mallery gabbro (labelled "M" in Fig. 1), with poorly exposed intrusive contacts, was initially interpreted as a monzodiorite (LeCheminant et al., 1981) due to the presence of modally significant potassium feldspar. Mapping in 2012, and subsequent petrographic and geochemical studies, demonstrated that the intrusion is a coarse augite-plagioclase gabbro with crude primary layering (mainly due to sorting of augite: Fig. 3a) that was infiltrated by a younger granitic melt along fractures and grain boundaries (Fig. 3b, insert). The gabbro includes metre-scale patches of coarse anorthosite (Fig. 3b) which strongly resemble the anorthosite of the Fish intrusion (Fig. 3c). The outcrop is cut by plagioclase-phyric diabase correlated with the McRae Lake dyke swarm (Fig. 3b). Additional dyke segments are imaged north and northwest of the outcrop in aeromagnetic anomaly maps.

In thin section, the gabbro is seen to be an augite-plagioclase-magnetite cumulate with substantial intercumulate hornblende (also partially replacing augite), plagioclase, alkali feldspar, apatite, opaques, and minor quartz. Electron

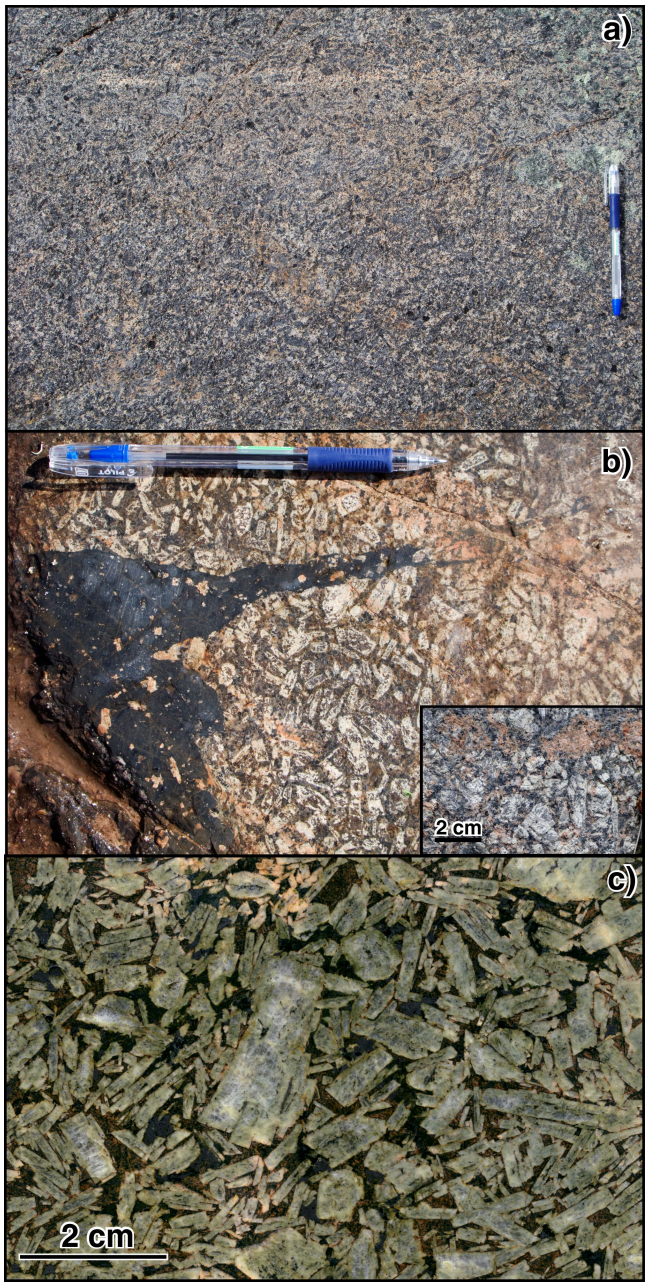

Figure 3. **a)** Augite-plagioclase gabbro of the Mallery complex. Note the modal variation (decreasing augite upwards) capped by a thin leucocratic layer, followed by a second augite-rich zone. 2014-003. **b)** Anorthositic gabbro patch within Mallery gabbro, cut by an apophysis of a McRae Lake diabase dyke. Inset shows invasion by younger granite between plagioclase laths, from the same outcrop. 2014–001. **c)** Polished slab from the Fish intrusion, with grey-green labradorite phenocrysts in a dark, chlorite-ilmenite matrix. 2014-002.

microprobe analyses (Table 1) revealed the presence of ilmenite, magnetite, and minor olivine (Fo_{46}). The average analyzed plagioclase composition is approximately An_{30}, but optical determinations indicate the cores of large euhedral plagioclase phenocrysts are up to An_{60}. Geochemical analyses (tabulated and discussed by Peterson et al., 2015) are within the range of alkali basalt, with a single Sm-Nd-depleted mantle model age (T_{DM}) of 2.36 Ga.

For comparison, microprobe analyses from the most magnesian Kivalliq basalt in the GEM-U database (04RAT-36A, south of Aberdeen Lake: Jefferson et al., in press) are included in Table 1. The Aberdeen basalt has olivine of composition Fo_{81} and also more magnesian clinopyroxene and more calcic plagioclase; however, Sm-Nd analyses indicate that the Mallery gabbro underwent less crustal contamination (*see* Discussion). This emphasizes that the intrusive gabbro underwent significant differentiation, consistent with the presence of modal layering and anorthositic plagioclase cumulates.

Granite intrusion

The granite forming the core of the Mallery complex was studied and described by Scott (2012). It is exposed primarily at two topographic high points, where it is orange-pink to orange-red weathering and porphyritic (plagioclase, sanidine, and quartz) with a medium- to fine-grained matrix containing graphic quartz-alkali feldspar intergrowths. It contains numerous dark green, 1 to 2 mm chlorite-rich clots, interpreted as altered microxenoliths of basaltic rock. Miarolitic cavities partially filled with quartz and blue/purple fluorite are common. The strongly porphyritic texture with open, mineralized cavities indicates rapid crystallization at low pressure, and we interpret the hilltop exposures as having crystallized close to the roof of the complex.

Contact metamorphism and epithermal mineralization

The southwest to south-southeast margin of the Mallery complex provides limited exposures of the country rocks to the complex (pre-2.1 Ga Marjorie Hills assemblage: Tschirhart, 2014) that are within tens of metres of the unexposed contact. The Marjorie Hills assemblage in this area is dominated by quartzofeldspathic gneiss with minor amphibolite, and two varieties of muscovite-bearing granite.

A shoreline exposure close to the core granite body consists of recrystallized amphibolite and granitic gneiss (the latter in boulders only) cut by narrow dykes of granite and plagioclase-phyric diabase. The amphibolite was affected by contact metamorphism, with dehydration reactions resulting in an assemblage of clinopyroxene+plagioclase+magnetite+titanite, plus an unidentified calc-silicate occurring as rounded porphyroblasts (scapolite?) (Fig. 4a). The resulting rock is strongly layered parallel to the original fabric of the amphibolite with varying modal amounts of pyroxene/magnetite and plagioclase that overprint previous deformation.

On the southwest margin of the granite, shards of similar amphibolite are present in an outcrop of quartz-rich breccia linked to formation of quartz-fluorite epithermal veins

Table 1. Electron microprobe analyses

Mineral	F	F	A	C	C	O	O	M	M	I	I
Sample	AB	MG	MG	AB	MG	AB	MG	AB	MG	AB	MG
n	9	8	6	9	10	1	7	6	5	4	5
X	An_{50}	An_{31}				Fo_{81}	Fo_{46}				
SiO_2	55.07	59.80	44.63	49.40	50.67	56.17	51.26	0.02	0.05	0.05	0.00
TiO_2	na	na	1.48	1.65	0.40	0.03	0.11	13.69	9.27	44.57	49.29
Al_2O_3	27.22	24.50	7.59	3.45	1.51	1.67	0.66	3.23	1.48	0.11	0.09
FeO	0.75	0.39	18.80	11.22	16.29	10.73	30.62	76.20	84.38	52.89	49.17
MnO	na	na	0.39	0.40	0.63	0.00	1.24	0.62	0.38	1.13	1.10
MgO	na	na	10.86	14.79	10.67	25.09	14.57	0.04	0.05	0.02	0.40
CaO	10.37	6.50	11.39	19.28	19.97	0.65	1.15	0.04	0.03	0.12	0.01
Na_2O	5.39	6.59	1.83	0.39	0.43	0.01	0.03	na	na	na	na
K_2O	0.66	1.96	1.28	0.01	0.13	0.03	0.03	na	na	na	na
P_2O_5	na	na	0.03	na	na	na	na	na	na	na	na
F	na	na	1.44	na	na	na	na	na	na	na	na
CL	na	na	0.41	na	na	na	na	na	na	na	na
SrO	0.18	0.12	na	na	na	na	na	na	na	na	na
BaO	0.13	0.17	0.02	na	na	na	na	na	na	na	na
V_2O_3	na	na	0.04	na	na	na	na	0.54	0.37	0.27	0.22
Cr_2O_3	na	na	na	na	na	na	na	1.86	0.04	0.00	0.03
total	99.8	100.0	100.2	100.6	100.7	94.4	99.7	96.2	96.1	99.1	100.3

na=not analyzed.

Minerals: F=feldspar, A=amphibole, C=clinopyroxene, O=olivine, M=magnetite, I=ilmenite.

Samples: AB=basalt south of Lake Aberdeen, MG=Mallery gabbro (12PHA-03). Analyses by K. Venance.

(Fig. 4b), with the development of coarse wollastonite at basalt-quartz contacts. Additional occurrences of wollastonite (Burton, 1981) and other skarns associated with the contacts of Nueltin granite bodies (Roberts, 1981) are widely distributed throughout the map area (Fig. 1; Peterson et al., 2014).

The south to southwest margin of the complex is the site of one of the larger and best-exposed occurrences of low-sulphidation epithermal quartz-fluorite mineralization identified by Biczok (1996). The outcrops consist of veins up to 2 m wide comprising multiple generations of laminated agate and massive to vuggy quartz, with purple fluorite. Nearby Nueltin Granite subcrop contains abundant, decimetre-scale miarolitic quartz-fluorite cavities. A polished surface of a sample collected from this area (sample 10PHA-01, Fig. 5) shows multiple episodes of agate-adularia precipitation, brecciation, and younger quartz-fluorite precipitation along fractures.

The agate likely is a product of high-temperature colloidal-silica precipitation, which can be associated with Au (e.g. Jebrak et al., 1996). The epithermal zones identified by Biczok (1996) were studied by Turner (2000) and Turner et al. (2001), who determined that the adularia-agate material contained native Au and electrum. An Sm-Nd isochron age of ca. 1423 Ma was obtained from single-specimen and pooled fluorite by Turner et al. (2003). Our specimens contain monazite grains but these are too small (approx. 2 μm) to date.

The largest epithermal centre is located on the north edge of the Pitz Formation near an approximate contact with Baker Lake Group (Chalcedonic stockwork zone, marked "epithermal Au" in Figure 1). Surface samples at this site have Au contents up to 24 ppm over 30 m (Turner et al., 2001).

Geophysical modelling

Two ground gravity transects were conducted over the Mallery complex in July 2012 (Tschirhart; Fig. 6). The station spacing along transect lines averaged 300 m. A LaCoste and Romberg model G metre G0431 was tied to the Canadian Gravity Standardization Net through the Baker Lake, Nunavut gravity base station, with a reading resolution of 0.01 mGal. The vertical and horizontal locations were calculated by differential GPS using a ProMark GPS and computed using GNSS Solutions. An elevation accuracy of better than 7 cm was determined for all measurements. The ground gravity data were corrected for latitude, instrument

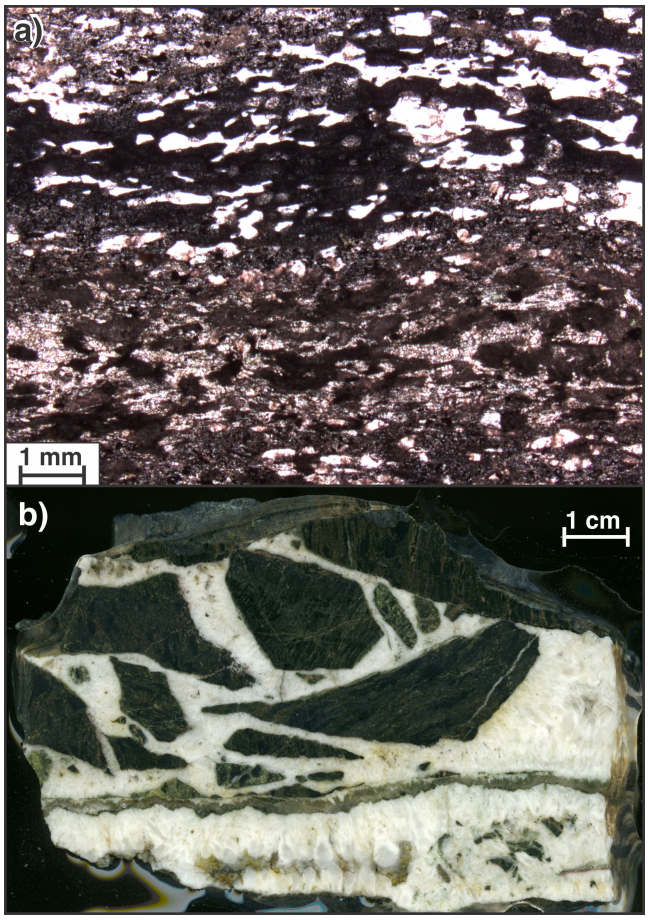

Figure 4. Contact metamorphic rocks from the margin of the Mallery complex. **a)** Photomicrograph of amphibolite, with a quasi-igneous assemblage of clinopyroxene, plagioclase, magnetite, and titanite produced by dehydration recrystallization (sample 10PHA-J07A2). 2015–013. **b)** Brecciated amphibolite in epithermal quartz. Coarse wollastonite is adjacent to the basalt fragments (sample 10PHA-J04). 2015-014.

drift, elevation and the Earth's tides, followed by the free air correction and Bouguer reduction. No terrain corrections were made as relief across the complex varies by less than 75 m. A regional gravity grid comprising 12 to 15 km spaced stations was acquired from the Canadian Geoscience Data Repository. Values interpolated from this grid were subtracted from each profile line, to calculate the residual signal free of the long-wavelength basement components. These data were used in all subsequent modelling.

The aeromagnetic data used in this study were extracted from the Canadian Geoscience Data Repository. Flight lines within the study area are spaced 800 m and gridded to 200 m using minimum curvature. For this study the grid was upward continued 5000 m and subtracted from the original grid to produce a residual image accentuating short wavelength near surface features, and removing the long-wavelength background signal that is not under consideration in the modelling. The aeromagnetic profiles used in the forward modelling were sampled from this grid along

Figure 5. Adularia-rich epithermal agate sample, showing multiple episodes of brecciation and silica precipitation (sample 10PHA-01). Adularia occurs as orange (Fe-stained) stringers and sub-millimetre sized euhedral wedges (not visible) in early agate. Purple fluorite is present as late fracture filling. 2015-015.

the ground gravity lines. GM-SYS Solutions™ software was used to compute the forward models beginning with a set of polyhedra, with the station topography input as the top surface, that were iteratively modified to obtain the best fit between the observed and computed gravity and magnetic signals. The geometry of the polyhedra are based on the known geology and petrophysical measurements of ground samples (magnetic susceptibility, density). As it was possible to adequately model the magnetic data with induced field magnetization controlled by known susceptibility values, remanence was assumed to not be present in the magnetic units. The root mean square (RMS) error was kept <10 nT and <0.5 mGal for magnetics and gravity cases.

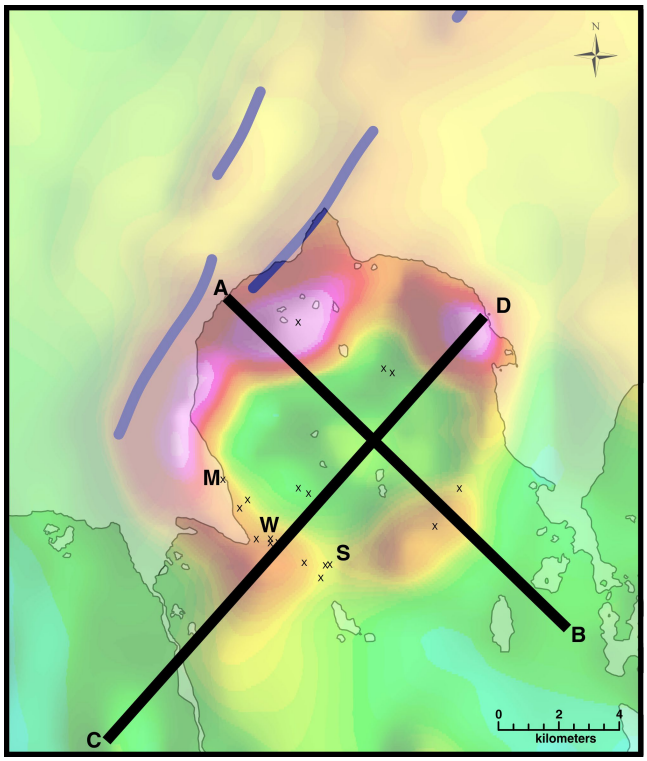

Figure 6. Aeromagnetic map of the Mallery complex, showing gravity survey lines. Line ends are keyed to Figure 7. Blue curves are interpreted dykes of the McRae Lake swarm. "x" = outcrop location (*see* Fig. 1 for geology). Contact metamorphic rock outcrops: M = recrystallized amphibolite; W = amphibolite in epithermal breccia with quartz/wollastonite; S = granite veins and gneiss.

The modelling results (Fig. 7) are consistent with a core of Nueltin Granite surrounded by a gabbroic collar of variable width, extending to a depth of approximately 1 km. However, there are no outcrops or subcrops of gabbro along the south edge of the complex, and it is likely that some of the magnetic signature there is due to magnetite generated by contact metamorphism in amphibolite and gneisses of the MHA. A gabbroic ring on the south side, if it exists, does not intersect the current level of erosion. A similar magnetic annulus, not exposed in outcrop, is present at the north tip of a rapakivi granite intrusion in central 65-O (Fig. 1).

Our modelling also indicates that the Mallery complex is underlain at about 1 km depth by dense rock with the properties of gabbro, which thickens and shallows to 400 m depth to the southwest, in the direction of the large exposure of Pitz Formation rhyolite. This may represent a sill complex that is the source of the gabbro collar, or may be related to older volcanic rocks (e.g. Christopher Island Formation). The model cross-sections are consistent with a granite-gabbro ring structure, such as those observed in some Phanerozoic anorogenic granite provinces (e.g. Nigeria: Bonin, 1986). The geometry of the Mallery complex, including a partially exposed gabbro collar, resembles that of the Proterozoic gabbro-rapakivi granite Ahvenisto Complex of Finland (Alviola et al., 1999).

Fish anorthosite intrusion

The Fish intrusion ("F," Fig. 1), 19 by 4 km, was emplaced along a basin-bounding fault of the Christopher Island Formation. Sampled exposures consist of packed, green-weathering, euhedral plagioclase phenocrysts to 8 cm, aligned parallel to the long axis of the intrusion, in a dark green matrix (Fig. 4c). The matrix has a distinctive mineral assemblage of clinopyroxene, largely replaced by single crystals of ilmenite studded with apatite, set in dark green chlorite containing dendritic needles of apatite+ilmenite (Fig. 8a). The intrusion is cut by quartz-feldspar porphyry dykes correlated by mineralogy and texture with the Nueltin granites. One porphyry dyke, located just north of the intrusion, has been dated by U-Pb (zircon) (this paper). The Sm-Nd composition of the Fish intrusion (T_{DM} = 2.42 Ga) is similar to that of the Mallery gabbro (Peterson et al., 2015).

A Pb-Cu mineral occurrence at Spec Lake (Webb, 1981) is located 5 km north of the Fish intrusion. It consists of 5 to 6 en échelon lenses about 1.5 m wide and 9 m long with massive galena, chalcopyrite, and bornite with minor digenite, enargite, chalcocite, sphalerite, tetrahedrite and others, including native Cu-Ag. A Pb-Pb (galena) model age of 1.77 to 1.8 Ga (depending on sample and specific lead evolution model) led Webb to correlate formation of the occurrence with ca. 1.75 Ga Nueltin Granite emplacement. A thin dyke-like extension of the intrusion to the northeast is similarly flanked on both sides at a 5 km distance by smaller Pb-Cu showings ('TEB 1-18' and 'Tebesjuak Lake' showings: Peterson et al., 2014). An (unexposed) extrapolation of this extension an additional 5 km across a small lake would terminate at outcrops of basalt (below).

Basalts in Pitz Formation

A group of basaltic outcrops at a topographic high near a Mackenzie diabase dyke ('B', Fig. 1) were initially targeted as potential sites of the Kuungmi Formation (1540 ± 10 Ma; Chamberlain et al., 2010) or as volcanic flows related to the Mackenzie dyke swarm (1267 Ma: LeCheminant and Heaman, 1989). After field study in 2010 and analysis (Scott, 2012), they were reinterpreted as basalts within the Pitz Formation. A glacially polished outcrop protected from erosion by the Mackenzie dyke consists of grey-brown to blue-black weathering rock with abundant centimetre- sized vesicles filled with epidote and silica. Sparse, slender white plagioclase phenocrysts up to 1 cm long, sometimes in glomeroporphyritic rafts, are present at <5 vol %. In discriminant diagrams, analyses plot as alkali basalt and are similar to the Mallery gabbro and Fish intrusion (Peterson et al., 2015).

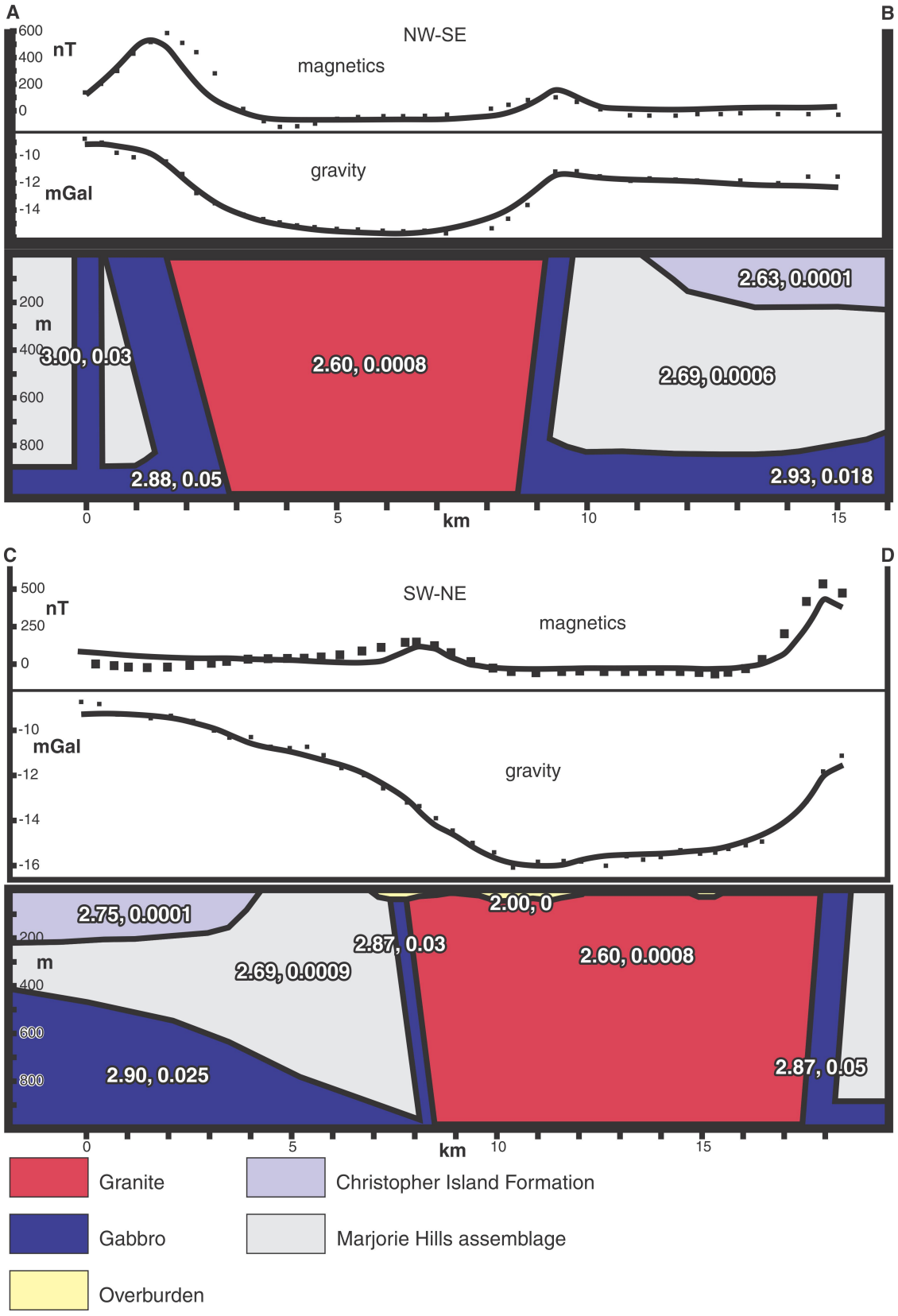

Figure 7. Gravimetric-magnetic interpretive model cross-sections through the Mallery complex. CI Fm = Christopher Island Formation.

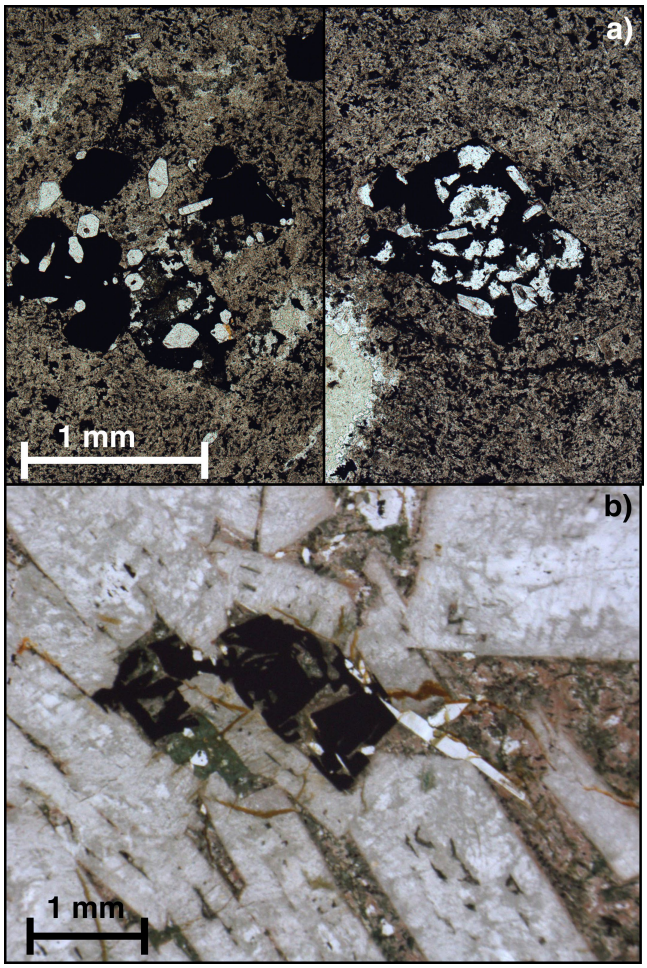

Figure 8. **a)** Ilmenite-apatite microxenoliths in two areas of a basaltic lava (sample 10PHA-J06) (photomicrograph, plane-polarized light). Note the euhedral pseudomorphs of clinopyroxene in the left-hand image. 2015-016. **b)** Ilmenite pseudomorphs of clinopyroxene with apatite between plagioclase laths, Fish intrusion (plane-polarized light) (sample 79LAAT-204). Green is chlorite. 2015-017.

Additional chocolate-brown-weathering basalt and mixed basalt/rhyolite volcaniclastic rocks were located 200 m north and several metres vertically below the high outcrop. A homogeneous, melanocratic sample (10PHA-J06) has T_{DM} = 2.41 Ga, nearly identical to the Fish anorthosite (Peterson et al., 2015). The groundmass of this sample contains numerous microxenoliths of ilmenite+apatite, including euhedral ilmenite replacement of clinopyroxene (Fig. 8b). These xenoliths resemble ilmenite pseudomorphs and apatite-ilmenite intergrowths in the intercumulate matrix of the Fish intrusion anorthosite. As the basalts are on strike with the northeast extension of the Fish intrusion, we surmise that related magmas formed the basalt outcrops, and were probably erupted from a subsurface extension of the intrusion.

McRae Lake dyke

Descriptions of the geology and petrography of the McRae Lake dyke ("MLD," Fig. 1) are in Tambosso (1981) and LeCheminant et al. (1981). Geochemical analyses (Peterson et al., 2015) indicate the dyke is distinctive from the Mallery gabbro, the Fish intrusion, and the basalts, but compositionally similar to samples of the McRae Lake dyke swarm, including basalts from the Aberdeen Lake area and dykes on the west side of Dubawnt Lake. All of these have a subalkaline basalt composition. Three Sm-Nd isotope analyses of McRae Lake dyke swarm samples yield an average T_{DM} of 2.62 Ga (Peterson et al., 2015).

The McRae Lake dyke is a 23 by 1.8 km, composite mafic intrusion that trends 035° (LeCheminant et al., 1980). It intrudes all exposed rocks it is in contact with, including quartz-feldspar porphyry dykes and a rapakivi intrusion at its south end. However, mafic-felsic mingling features are present within the dyke in that area (LeCheminant et al., 1980; Tambosso, 1981). The dyke has two main phases, a medium-grained, grey-green, plagioclase-phyric gabbro (predominant to the southwest) and a grey- to red-weathering plagioclase glomeroporphyritic, quartz monzodiorite to diorite that intruded axially down the length of the gabbro. The gabbro displays chilled margins at all contacts, and at the southwest end contains xenoliths of rapakivi granite and recrystallized orthogneiss or metasediment. The monzodiorite has both sharp and gradational contacts with the gabbro; clinopyroxene-rimmed quartz xenocrysts are a common feature (Tambosso, 1981). All samples have a similar mineral assemblage, with laths of zoned plagioclase (labradorite to andesine) up to 6 mm in length with subordinate alkali feldspar, quartz, and altered clinopyroxene grains in a micrographic matrix. Internal contact relationships are consistent with multiple episodes of magma emplacement, with a clear mafic to felsic progression (Tambosso, 1981).

The McRae Lake dyke coincides with a strong aeromagnetic signature, which is cut off abruptly to the northeast by a northwest-trending east-side-down normal fault (Tambosso, 1981). Narrow, discontinuous, north-northeast-trending linear aeromagnetic highs northeast of the fault indicate that dykes related to the gabbro extend to Mallery Lake and beyond. Narrow, plagioclase-phyric dykes are exposed on the shoreline of Mallery Lake and cut the Mallery Lake gabbro. The north-northeast-trending dykes in map area 65-O are interpreted to be part of the regionally extensive north-northeast-trending McRae Lake dyke swarm (Buchan and Ernst, 2013). Another swarm of buried east-northeast-trending diabase dykes is traced north of Tebesjuak Lake using aeromagnetic signatures from high-resolution geophysics contributed by Bayswater Uranium Corporation as part of the Geophysical Compilation and Interpretation, Northeastern Thelon Basin Region consortium agreement (Tschirhart et al., 2011). These dykes are assigned to the Thelon River swarm of Buchan and Ernst (2013).

Pamiutuq intrusion and rhyolite porphyry dykes

The Pamiutuq intrusion ("P" in Fig. 1; LeCheminant et al., 1979a, 1980) is a 700 km^2, near-circular subvolcanic lopolith composed primarily of pink- to red-weathering, feldspar porphyritic granite with microperthitic orthoclase, plagioclase, and quartz phenocrysts set in a fine-grained granophyric matrix. Booth (1983) described plagioclase-phyric mafic blebs with cuspate chilled margins containing plagioclase megacrysts to 5 cm and concluded that the intrusion exhibits strong evidence of comingling with mafic magma. Accessory phases are chloritized biotite, magnetite, ilmenite, apatite, and zircon. Xenoliths are distributed widely throughout the pluton, and include granitoid gneiss, mafic hornblende syenite, and texturally contrasting varieties of granite.

The main pink to red phase of the Pamiutuq granite passes upward and laterally into a finer grained purple-weathering porphyritic chilled margin, typically less than 100 m wide, that cuts the surrounding rocks discordantly. Along the northwestern contact the purple border phase is up to 4 km wide, where it is interpreted as the shallowly dipping upper contact of the granite intruded into and beneath slightly older rhyolite successions. Intrusive contacts with Pitz rhyolites were recognized locally, although continuous gradations between flow-banded rhyolite and purple porphyry were also noted. Field relations indicate intrusion of the Pamiutuq granite preceded that of elongated intrusions of rapakivi granite to the west and northwest (Fig. 1; LeCheminant et al., 1980).

GEOCHRONOLOGY

Mallery gabbro (U-Pb baddeleyite)

Sample 12PHA-03B, a mesocratic gabbro, was selected for U-Pb dating on the basis of coarse texture, absence of visible granitic veins or patches, and relative lack of alteration (Fig. 9a). However, the sample contains complex single crystals and clusters of zircon (dendritic, or hopper-textured), and zircon coronas around some baddeleyite grains (Fig. 9b), that are interpreted as products of thermal metamorphism/metasomatism related to the granite.

Analytical method

The sample was processed in the Jack Satterly Geochronology Lab at the University of Toronto. Conventional crushing and grinding techniques (jaw crusher and disc mill) were employed, followed by a shaking water Wilfley table procedure to obtain a heavy mineral concentrate, and finally by Frantz magnetic and methylene iodide heavy-liquid separations. Three fractions of baddeleyite, comprising 5 grains each, were selected for U-Pb analysis. Baddeleyite grains were washed on parafilm and loaded

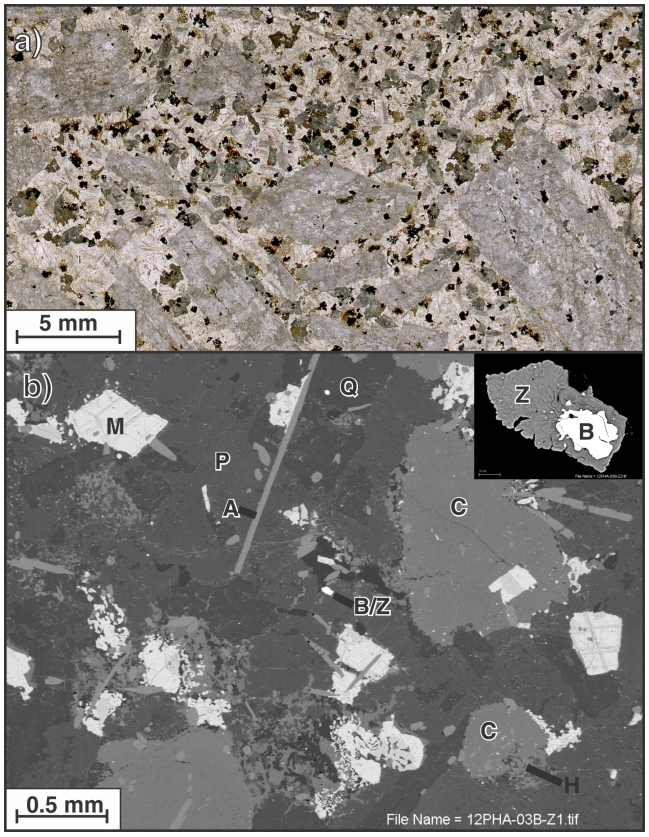

Figure 9. Mallery gabbro. **a)** Photomicrograph of relatively leucocratic gabbro (sample 12PHA-03B) showing centimetre-scale plagioclase and smaller clinopyroxene (green; partially replaced by brown hornblende) and magnetite/ilmenite (black) in a quartz-feldspar matrix. 2015-018. (b) Backscattered electron image of gabbro, with a central baddeleyite-zircon grain (B/Z). Inset is a magnified and enhanced view of this grain showing partial replacement of central baddeleyite by a thick rim of zircon. M = magnetite, Q = quartz, P = plagioclase feldspar, A = apatite, C = clinopyroxene, H = hornblende. 2015-019.

into Teflon bombs with concentrated HF along with a mixed ^{205}Pb – ^{235}U isotopic tracer solution (Krogh, 1973). Dissolution occurred over three to four days at 195°C, after which fractions were dried down with phosphoric acid and loaded with silica gel directly onto outgassed rhenium filaments. Larger grain dissolutions were passed through ion exchange columns to obtain purified elutions of Pb and U. The isotopic compositions of Pb and U were measured using a single Daly collector with a pulse counting detector on a solid source VG354 mass spectrometer. A detector mass discrimination of 0.053% per atomic mass unit (AMU) and a dead time of 20 nsec were employed for Daly detector measurements. A thermal-source mass-discrimination correction of 0.1% per atomic mass unit was applied for both Pb and U. The assigned laboratory blank for U was 0.2 pg, while that for Pb is routinely measured below 1 pg. Error estimates were calculated by propagating known sources of

analytical uncertainty for each analysis including within-run ratio variability, uncertainty in the fractionation correction, and uncertainties in the isotopic composition of laboratory blank.

Uncertainties for the ID-UMS data are given at the 95% (2σ) confidence level. Initial corrections were made using an in-house data reduction program (UTILAGE). Decay constants used in age calculations are those of Jaffey et al. (1971). Graphical data presentation and quoted ages were generated using the Microsoft Excel Add-in IsoplotEx v. 3.00 of Ludwig (2003).

Results

All three fractions analyzed are either concordant or near-concordant (0.3–11% discordant: Table 2, Fig. 10). Calculated Th/U ratios (0.02–0.06) are typical for baddeleyite. Model $^{207}Pb/^{206}Pb$ ages scatter between ca. 1760–1770 Ma: 1769 ± 6 Ma (Bd-1), 1762 ± 4 Ma (Bd-2), and 1758 ± 8 Ma (Bd-3). The younger $^{207}Pb/^{206}Pb$ ages may result from partial Pb-loss during secondary zircon overgrowth, perhaps due to emplacement of the adjacent Nueltin Granite body (1755.4 ± 1.8 Ma, U-Pb zircon: Turner et al., 2003).

The concordia diagram presents data for one additional baddeleyite fraction (Bd-4) separately analyzed after the first three. Two age interpretations are possible due to the limited number of points and slight scatter. The most concordant analysis of 1769 ± 6 Ma (which straddles concordia; 0.33% discordant) is equivalent to the upper intercept of a regression though that point and the origin (solid line), and is the interpreted crystallization age of the gabbro. Regression #2 (dashed line) includes the three points Bd-1, -2 and -4, which has a lower intercept age near 850 Ma (possibly representing an age of secondary Pb loss) and an upper intercept age of 1772 ± 5 Ma. The $^{207}Pb/^{206}Pb$ age for fraction Bd-3 is 1758 ± 8 Ma, and it is also very nearly concordant; it is interpreted as affected by resetting during intrusion of the adjacent Nueltin Granite.

McRae Lake dyke (U-Pb baddeleyite)

The McRae Lake gabbro (sample 80LAA-W37–1) contains moderately altered plagioclase and pale green clinopyroxene phenocrysts partially altered to amphibole that are zoned with strongly blue-green pleochroic, sodic rims. These are set in a potassium feldspar-quartz granophyre with Fe-Ti oxides, apatite, biotite, baddeleyite, and zircon. Baddeleyite is mostly enclosed in amphibole and biotite. Recovered baddeleyite grains were deep brown, well faceted, tabular euhedral crystals and fragments, averaging 100 μm long. A total of three fractions (Bd1A, Bd1B, and Bd1C) were picked, each containing two clear, inclusion-free and unaltered grains for analysis.

Analytical method

Separation of baddeleyite at the GSC geochronology lab followed conventional techniques for crushing, Wilfley table concentration, heavy liquid density separation, and isolation using a Frantz™ isodynamic magnetic separator. Thermal ionization mass spectrometry, isotope dilution procedures for U and Pb isotopic analysis (ID-TIMS) are described in Parrish et al. (1987). Crystals selected for analysis were grouped based on quality, determined primarily by uniform colour and absence of turbidity, fractures, inclusions, and attached grains. Treatment of analytical uncertainties and their propagation is based on procedures outlined by Roddick (1987). Common Pb corrections use Pb-isotope model compositions of Stacey and Kramers (1975). Total analytical blanks for Pb and U during this study were typically <1 pg and <0.1 pg. Uranium and Pb isotopic ratios were measured using a Triton mass spectrometer operated in either static multi-collection mode or using a secondary electron

Table 2. U-Pb (baddeleyite) data, Mallory gabbro (sample 12PHA-03B)

Fraction	U (ppm)	PbT (pg)	Pbc (pg)	Th/U	$^{206}Pb/^{204}Pb$	$^{206}Pb/^{238}U$	$^{207}Pb/^{235}U$	$^{207}Pb/^{238}U$	$^{206}Pb/^{238}U$ age	$^{207}Pb/^{235}U$ age	$^{207}Pb/^{206}Pb$ age	disc,%
Bd-1	392	11.94	0.5	0.058	1611	0.314739 ± 0.001723	4.69475 ± 0.03126	0.108184 ± 0.000361	1764 ± 8.4	1766.3 ± 5.6	1769.1 ± 6.1	0.3
Bd-2	469	14.06	0.36	0.043	2600	0.311064 ± 0.00092	4.62318 ± 0.01827	0.107793 ± 0.000247	1745.9 ± 4.5	1753.5 ± 3.3	1762.4 ± 4.2	1.1
Bd-3	493	14.76	0.84	0.019	1190	0.312811 ± 0.000994	4.63451± 0.02838	0.107522 ± 0.000491	1753.5 ± 4.9	1755.5 ± 5.1	1758.8 ± 8.4	0.3

All three fractions contained 5 medium brown subhedra of baddeleyite.
Quoted errors are 2 standard deviations.
PbT is total Pb in picograms.
Pbc is total measured common lead in picograms, assuming the isotopic composition of laboratory blank: 206/204 = 18.221; 207/204 = 15.612; 208/204 = 39.360 (errors of 2%).
Pb/U atomic ratios are corrected for spike, fractionation, blank, and where necessary initial common Pb; 206/204 is corrected for spike and fractionation.
Th/U is model value calculated from radiogenic $^{208}Pb/^{206}Pb$ ration and $^{207}Pb/^{206}Pb$ age, assuming concordance.
U decay constants are from Jaffey et al. (1971).

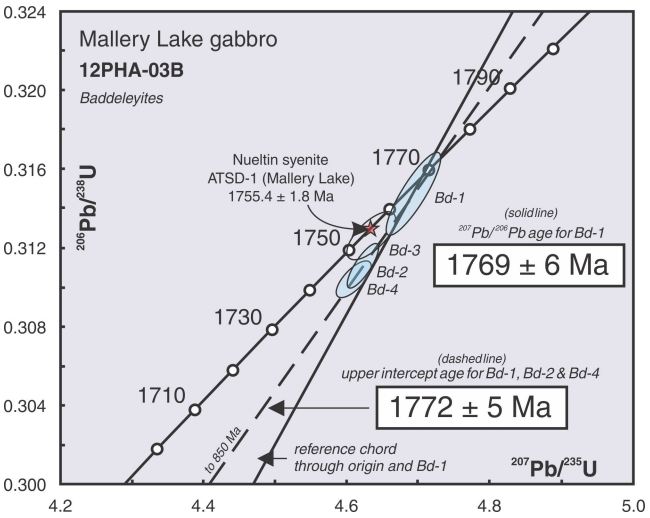

Figure 10. Concordia diagram for Mallery gabbro baddeleyite.

multiplier and ion-counting system. The ^{205}Pb, ^{206}Pb, ^{207}Pb, and ^{208}Pb isotopes were measured simultaneously in Faraday collectors, with ^{204}Pb in an axial secondary electron multiplier. Mass fractionation was corrected for Pb, by applying a 0.09%/amu. Concordia diagrams and weighted mean plots were generated using Isoplot 3.0 (Ludwig, 2003). Concordia ellipse errors and weighted mean errors are shown on Figure 11 at the 2σ (95% confidence) level of uncertainty.

Results

The results from the three fractions are weakly discordant (ca. 1%, Table 3, Fig. 11). Linear regression through the data yields a discordia line with an upper intercept at 1751 Ma. The weighted ^{207}Pb/^{206}Pb average is 1753.6 ± 1.2 Ma (mean standard weighted deviates [MSWD] = 0.22). These data are consistent with results from the same sample originally analyzed by TIMS by Roddick and LeCheminant (unpub. data, Table 3), which were more discordant and had a slightly younger ^{207}Pb/^{206}Pb age of 1750 ± 6 Ma. Our results, which are the least discordant, yield a more precise ^{207}Pb/^{206}Pb age of 1753.6 ± 1.2 Ma which is interpreted as the time of crystallization of the McRae Lake dyke.

Pamiutuq intrusion (U-Pb zircon)

Zircon crystals were obtained from archival separates of a sample of the main phase of the Pamiutuq granite intrusion (sample 78LAA-T209–1; zircon sample z476). Zircon ranging between 150 and 200 μm showed two texturally discrete populations, apparent in transmitted light. The dominant population were clear, colourless, and glassy in appearance with rare fracturing. A subordinate population of zircon typically appeared heavily fractured with minor staining, occurring as cores with overgrowths of the latter. Large fluid inclusions were common within both populations. In backscatter electron (BSE) images, the populations of zircon generally exhibited strong contrast in brightness, indicative of high U and Th content in the fractured population. The primary population of zircon shows faint and fine, continuous zoning commonly observed in Nueltin Granite zircons (van Breemen et al., 2005). The population of highly fractured zircons exhibit more discrete zoning, often interrupted by strong alteration, partially or wholly enclosed by fine, glassy and unaltered overgrowths. The overgrowths are fractured in a manner characteristic of expansion due to metamictization of U-rich cores.

Analytical method

Zircon was separated by standard techniques and mounted in an epoxy disc with fragments of the GSC standard 6266 (^{206}Pb/^{238}U = 559 Ma) and secondary standard 1242 (^{206}Pb/^{238}U = 2677.3 ± 3 Ma), then polished approximately to half grain thickness, and characterized by transmitted light microscopy and backscattered electron (BSE) images on scanning electron microscope. Polished mount surfaces were coated with 10 nm of high purity Au. A primary beam diameter of approximately 25 μm was used for ion-probe analyses (SHRIMP). The SHRIMP calibration using standards was performed according to Stern and Amelin (2003) with a measured uncertainty of 1.0% across each of the analytical sessions. Detailed analytical methods can be found in Stern (1997) and Stern and Amelin (2003) and results reported in Table 3. Concordia and mean standard of the weighted deviates (MSWD) diagrams were calculated at the 2σ level using the program Isoplot 3.0 (Ludwig, 2003). The mount sporadically produced higher common ^{204}Pb during the first analytical session, resulting in a slightly lower precision for that data. The mount was cleaned and recoated, with a noticeable effect on reduced common ^{204}Pb.

Results

Analysis indicates there are two populations which contrast significantly in total Th and U, but Th/U ratios (average 0.9) are indistinguishable (Table 4). The analyses of 31 zircons are concordant to weakly discordant with one strongly discordant (+7%) analysis (29.1) (Fig. 12). If this sole analysis is removed, the remaining analyses give a concordia age of 1746.6 ± 5.3 Ma (95% confidence, mean standard weighted deviates [MSWD] = 6.7, probability of concordance 1%). This age overlaps within error of the weighted average ^{207}Pb/^{206}Pb age of 1752.6 ± 4.1 Ma (2σ, MSWD = 1.7; Fig. 12). The ^{207}Pb/^{206}Pb age represents the best estimate for the crystallization age of the Pamiutuq pluton. The data are consistent with an upper intercept for a linear regression of discordant TIMS data by Roddick and LeCheminant (unpublished data, 1987; Table 3). Age differences, if any, between the high U (ppm) metamict zircons and the primary population are irresolvable, and consistent Th/U ratios indicate they are antecrysts derived from the same melt undergoing fractionation.

Table 3. U-Pb (baddeleyite) data, McRae Lake dyke (sample 80LAA-W37-1, Z1201)

Fraction	wt (mg)	U (ppm)	Pb (ppm)	$^{206}Pb/^{204}Pb$	Pb,pg	$^{208}Pb/^{206}Pb$	$^{207}Pb/^{235}U$	$^{206}Pb/^{238}U$	$^{207}Pb/^{206}Pb$	$^{207}Pb/^{206}Pb$ Age (Ma)	$^{206}Pb/^{238}U$ Age (Ma)	$^{207}Pb/^{235}U$ Age (Ma)	Discord(%)
Bd1A	4	287	85	2335	9	0.01	4.576± 0.13%	0.3093± 0.09%	0.10731± 0.06%	1754±2	1737.1± 2.8	1744.9± 2.2	1.11
Bd1B	3	240	72	765	19	0.01	4.585± 0.21%	0.3100± 0.11%	0.10729± 0.15%	1754±6	1740.5± 3.4	1746.6± 3.5	0.87
Bd1C	3	1172	350	17550	3	0.01	4.586± 0.11%	0.3101± 0.09%	0.10726± 0.04%	1753±2	1741.4± 2.7	1746.8± 1.9	0.78
105(a)	103	1114	328	11113	200	0.01	4.530± 0.13%	0.3068± 0.12%	0.10708± 0.03%	1750±1	1725.0± 3.8	1736.5± 2.2	1.64
105(b)	148	1267	374	17776	205	0.01	4.534± 0.12%	0.3073± 0.11%	0.10702± 0.03%	1749±1	1727.3± 3.3	1737.3± 2.0	1.43

Quoted errors are 1 standard deviation except ages (2)
Bd1 fractions by TIMS (this study)
105 fractions by TIMS (Roddick and LeCheminant, unpublished data)

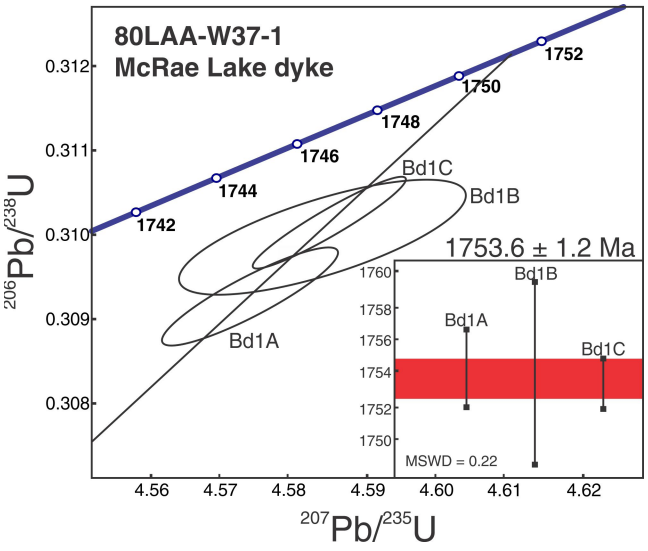

Figure 11. Concordia diagram and weighted average summary for McRae Lake dyke baddeleyite.

Quartz-feldspar porphyry dyke (U-Pb zircon)

Zircon crystals were obtained from archival separates (zircon sample z645) of one sample from a quartz feldspar porphyry dyke collected NE of the Fish intrusion (82LAA-T305–1). Zircons were typically 150 µm with a 4:1 length-to-width ratio, and ranged up to 300 µm and a 6:1 length-to-width ratio. In transmitted light the zircon population was clear, colourless and glassy in appearance with rare fracturing. Large fluid inclusions were common with variable reddish coloured staining. In BSE images, the zircons show faint and fine, continuous zoning. Faint zoning is consistent with relatively low totals and little variation in U (ppm) and Th (ppm) as the zircon crystallized, indicated by the consistent Th/U ratios between 1.09 and 0.51. Analytical procedures were the same as for the Pamiutuq zircons.

Analyses of 29 zircons show results that are concordant to weakly discordant (± 3; Table 4, Fig. 13), with a concordia age of 1739.2 ± 4.6 Ma (95% confidence, mean standard weighted deviates [MSWD] = 7.3, probability of concordance 0.7%). This age overlaps within error of the weighted average $^{207}Pb/^{206}Pb$ age of 1746.7 ± 4.3 Ma (2σ, MSWD = 0.96). The $^{207}Pb/^{206}Pb$ age represents the best estimate for the crystallization of the dyke. The data are also consistent with a linear regression of discordant TIMS results by Roddick and LeCheminant (unpublished data, 1987; Table 4).

DISCUSSION

As discussed by Peterson et al. (2015), the Mallery gabbro (which contains an anorthosite phase), the Fish anorthosite, and the nearby basalts are all of alkali gabbro composition, and have Nd model ages in the range 2.36 to 2.42 Ga, which are distinct from model ages of the subalkaline McRae Lake dyke and McRae Lake swarm dykes (ca. 2.62 Ga). There was therefore a change in primary magma composition within the Kivalliq Suite from alkaline to subalkaline basalt over about 15 million years. The bimodal Kivalliq Suite closely fits a generally accepted model for anorogenic (and particularly rapakivi-textured) granites wherein silicic melts are generated by ponding of juvenile basaltic magmas in the lower crust (*see* for example Haapala et al., 2005). Although some mixing occurs via mutual entrainment of both magma types during ascent to the surface, separate intrusions of granite and basalt are the norm, including diabase dyke swarms. No true primary mafic melts with juvenile isotopic compositions have yet been identified within the Kivalliq Suite, and all present samples probably represent mixtures of mantle melts with crustal melts. The span for Nueltin Granite emplacement (ca. 1740–1765 Ma) as determined by van Breemen et al. (2005), is approximately 25 Ma. Our age for the Mallery gabbro, near 1770 Ma, extends this to approximately 30 Ma.

Table 4. U-Pb SHRIMP data, Pamiutuq granite and quartz-feldspar porphyry dyke

Spot	#	U (ppm)	Th (ppm)	Th/U	Pb* (ppm)	$^{204}Pb/^{206}Pb$	$f(206)_{204}$	$^{208*}Pb/^{206*}Pb$	$^{207*}Pb/^{235}U$	$^{206*}Pb/^{238}U$	Corr.	$^{207*}Pb/^{206*}Pb$	$^{206}Pb/^{238}U$ age	$^{207}Pb/^{206}Pb$ age	%disc
476-1.1	1	93	83	0.93	24	2.27E-04±4.42E-05	3.17E-04	0.28805±0.00389	4.54840±0.06402	0.30658±0.00378	0.8752	0.10760±0.00073	1719±21	1759±12	2.29
476-4.1	1	43	35	0.85	11	4.63E-04±9.28E-05	1.21E-03	0.28127±0.00568	4.67340±0.07914	0.31034±0.00336	0.6395	0.10922±0.00142	1737±18	1786±24	2.81
476-5.1	1	67	42	0.64	18	3.70E-04±5.69E-05	1.23E-03	0.19652±0.00376	4.53344±0.06197	0.31290±0.00328	0.7672	0.10508±0.00092	1760±18	1716±16	-2.61
476-9.1	1	112	99	0.91	30	1.87E-04±3.84E-05	7.95E-04	0.27415±0.00347	4.55119±0.05438	0.30949±0.00319	0.8617	0.10665±0.00065	1738±18	1743±11	0.32
476-11.1	1	48	43	0.93	13	3.21E-04±7.23E-05	5.21E-04	0.29790±0.00849	4.61690±0.07321	0.30811±0.00364	0.7448	0.10868±0.00115	1726±20	1777±19	2.95
476-20.1	1	44	39	0.91	12	1.88E-05±6.58E-06	5.26E-05	0.37810±0.00199	4.63823±0.04996	0.31446±0.00334	0.9858	0.10698±0.00019	1764±19	1749±3	-0.92
476-21.1	1	46	39	0.89	13	2.37E-05±1.82E-05	1.46E-04	0.32962±0.00241	4.47556±0.04745	0.30213±0.00306	0.9559	0.10743±0.00033	1695±17	1756±6	3.53
476-22.1	1	55	47	0.87	15	4.19E-04±7.67E-05	1.13E-03	0.28478±0.00563	4.50476±0.07064	0.30610±0.00329	0.6854	0.10673±0.00122	1719±18	1744±21	1.50
476-24.1	1	47	36	0.79	13	2.11E-04±6.27E-05	5.69E-04	0.27524±0.00553	4.74661±0.06878	0.32027±0.00343	0.7398	0.10749±0.00105	1796±19	1757±18	-2.20
476-25.1	1	87	119	1.41	23	2.18E-04±9.29E-05	6.45E-04	0.26938±0.00496	4.55360±0.07687	0.31185±0.00333	0.6325	0.10590±0.00138	1752±18	1730±24	-1.31
476-26.1	1	60	47	0.82	16	3.78E-04±7.82E-05	1.06E-03	0.24742±0.00506	4.51146±0.07111	0.30874±0.00331	0.6795	0.10598±0.00123	1735±18	1731±21	-0.21
476-27.1	1	84	74	0.91	22	2.99E-04±4.93E-05	1.11E-03	0.43439±0.00504	4.55919±0.05876	0.31357±0.00326	0.8063	0.10545±0.00080	1763±18	1722±14	-2.39
476-32.1	1	37	29	0.81	10	2.81E-04±6.61E-05	8.84E-04	0.25904±0.00461	4.58807±0.06609	0.31222±0.00330	0.7327	0.10658±0.00104	1753±18	1742±18	-0.65
476-33.1	1	85	74	0.90	23	3.37E-04±4.86E-05	1.22E-03	0.27089±0.00403	4.58499±0.05888	0.31175±0.00324	0.8104	0.10667±0.00080	1750±18	1743±14	-0.40
476-34.1	1	34	24	0.72	9	1.48E-04±6.15E-05	6.15E-04	0.38632±0.00395	4.16682±0.05606	0.28605±0.00296	0.7686	0.10565±0.00091	1610±16	1726±16	6.81
476-35.1	1	68	71	1.07	18	4.77E-04±9.49E-05	1.18E-03	0.24329±0.00566	4.49113±0.07954	0.30964±0.00338	0.6161	0.10519±0.00147	1742±19	1718±26	-1.41
476-36.1	1	75	83	1.14	20	7.09E-05±2.70E-05	2.65E-04	0.27397±0.00398	4.66050±0.05410	0.31247±0.00324	0.8928	0.10818±0.00057	1751±18	1769±10	1.04
476-37.1	1	74	63	0.88	19	6.57E-04±1.08E-04	1.57E-03	0.24457±0.00584	4.59394±0.08703	0.31147±0.00343	0.5809	0.10697±0.00165	1748±19	1748±28	0.03
476-38.1	1	94	121	1.33	25	3.38E-04±5.93E-05	4.34E-04	0.32890±0.00483	4.52543±0.07027	0.30863±0.00393	0.8191	0.10635±0.00095	1733±22	1738±16	0.25
476-39.1	1	93	95	1.05	25	2.48E-04±4.48E-05	8.70E-04	0.34662±0.00478	4.54352±0.05753	0.30789±0.00321	0.8234	0.10703±0.00077	1728±18	1749±13	1.25
476-12.1	2	514	630	1.27	139	1.55E-04±6.06E-05	5.43E-04	0.28053±0.00433	4.61373±0.06282	0.30697±0.00321	0.7677	0.10901±0.00095	1719±18	1783±16	3.65
476-16.1	2	334	348	1.08	87	1.72E-04±4.10E-05	6.75E-04	0.41180±0.00465	4.58889±0.05600	0.31021±0.00321	0.8475	0.10729±0.00070	1740±18	1754±12	0.79
476-29.1	2	148	249	1.73	36	2.57E-04±4.14E-05	1.00E-03	0.31835±0.00408	4.63327±0.05679	0.31502±0.00326	0.8441	0.10667±0.00070	1768±18	1743±12	-1.45
476-63.1	3	55	47	0.88	15	-4.47E-07±-6.49E-07	-3.03E-06	0.34063±0.00162	4.52038±0.04611	0.30518±0.00308	0.9909	0.10743±0.00015	1712±17	1756±3	2.55
476-64.1	3	36	35	0.99	10	1.11E-04±6.69E-05	2.53E-04	0.25927±0.00482	4.62601±0.06813	0.31426±0.00345	0.7458	0.10676±0.00105	1764±19	1745±18	-1.10
476-65.1	3	76	68	0.91	20	1.29E-05±3.69E-05	1.17E-05	0.28896±0.00629	4.67690±0.07787	0.31178±0.00465	0.8961	0.10879±0.00080	1745±26	1779±13	1.92
476-66.1	3	28	55	2.04	7	5.27E-05±4.05E-05	1.39E-04	0.27618±0.00724	4.55029±0.05730	0.30866±0.00331	0.8511	0.10692±0.00071	1732±18	1748±12	0.88
476-67.1	3	81	71	0.91	22	2.06E-04±4.53E-05	3.32E-04	0.62065±0.01072	4.56996±0.06762	0.30858±0.00364	0.7975	0.10741±0.00096	1731±20	1756±16	1.44
476-69.1	3	60	56	0.96	16	3.44E-05±1.27E-05	6.56E-05	0.28591±0.00417	4.64489±0.05595	0.31169±0.00352	0.9380	0.10808±0.00045	1746±20	1767±8	1.18
476-70.1	3	68	93	1.40	18	1.47E-04±4.07E-05	3.52E-04	0.28443±0.00480	4.42794±0.05719	0.30534±0.00332	0.8408	0.10518±0.00074	1718±18	1717±13	-0.02
476-47.1	4	583	641	1.14	153	8.09E-05±4.20E-05	2.04E-04	0.42269±0.00561	4.50493±0.05770	0.30704±0.00331	0.8423	0.10641±0.00073	1724±18	1739±13	0.84

82LAA-T305-1, Quartz feldspar porphyry dyke
Notes (*see* Stern, 1997)
Spot name follows the convention x-y.z; where x = sample number, y = grain number and z = spot number. Multiple analyses in an individual spot are labelled as "x-y.z.z"
Uncertainties reported at 1s (absolute) and are calculated by numerical propagation of all known sources of error.
$f(206)_{204}$ refers to mole fraction of total ^{206}Pb that is due to common Pb, calculated using the ^{204}Pb-method; common Pb composition used is the surface blank (4/6: 0.05770; 7/6: 0.89500; 8/6: 2.13840)
* refers to radiogenic Pb (corrected for common Pb)
Discordance relative to origin = 100 * (($^{207}Pb/^{206}Pb$ age -$^{206}Pb/^{238}U$ age)/($^{207}Pb/^{206}Pb$ age))
Error in $^{206}Pb/^{238}U$ calibration 1%
Th/U calibration: F = 0.03900*UO + 0.85600

Table 4. (cont.)

Spot	#	U (ppm)	Th (ppm)	Th/U	Pb* (ppm)	$^{204}Pb/^{206}Pb$	$f(206)_{204}$	$^{208*}Pb/^{206*}Pb$	$^{207*}Pb/^{235}U$	$^{206*}Pb/^{238}U$	Corr.	$^{207*}Pb/^{206*}Pb$	$^{206}Pb/^{238}U$ age	$^{207}Pb/^{206}Pb$ age	%disc
645-1.1	1	41	37	0.93	11	5.71E-04±1.16E-04	1.46E-03	0.31273±0.00620	4.48384±0.08755	0.30355±0.00332	0.5597	0.10713±0.00173	1704±18	1751±30	2.75
645-2.1	1	39	28	0.76	10	3.94E-04±1.16E-04	8.69E-04	0.24463±0.00567	4.60459±0.09031	0.31078±0.00347	0.5693	0.10746±0.00173	1743±19	1757±29	0.79
645-3.1	1	53	42	0.83	14	2.39E-04±7.39E-05	3.39E-04	0.24238±0.00488	4.53492±0.07462	0.30993±0.00381	0.7474	0.10612±0.00116	1741±21	1734±20	-0.43
645-4.1	1	65	46	0.73	17	3.84E-04±6.64E-05	9.95E-04	0.23273±0.00428	4.49230±0.06565	0.30712±0.00331	0.7377	0.10609±0.00105	1726±18	1733±18	0.44
645-6.1	1	60	60	1.05	16	1.56E-04±7.35E-05	1.60E-04	0.31213±0.00519	4.47260±0.08807	0.30641±0.00429	0.7114	0.10587±0.00147	1722±24	1729±25	0.42
645-7.1	1	78	60	0.80	21	1.96E-04±4.79E-05	6.92E-04	0.24005±0.00392	4.57779±0.05852	0.30715±0.00320	0.8155	0.10810±0.00080	1721±18	1768±14	2.64
645-9.1	1	94	79	0.87	25	2.09E-05±2.98E-05	6.54E-05	0.25811±0.00373	4.60734±0.05433	0.30845±0.00324	0.8912	0.10834±0.00058	1728±18	1772±10	2.48
645-10.1	1	85	60	0.73	23	2.50E-04±5.42E-05	9.25E-04	0.22515±0.00362	4.55202±0.06004	0.31070±0.00323	0.7886	0.10626±0.00086	1745±18	1736±15	-0.52
645-12.1	1	84	50	0.61	22	2.27E-04±4.35E-05	8.23E-04	0.19487±0.00345	4.53690±0.05675	0.30686±0.00319	0.8315	0.10723±0.00075	1722±18	1753±13	1.80
645-14.1	1	55	45	0.86	15	5.07E-04±8.20E-05	1.48E-03	0.26475±0.00502	4.60889±0.07344	0.31266±0.00334	0.6696	0.10691±0.00127	1755±18	1747±22	-0.42
645-15.1	1	97	65	0.69	25	1.67E-04±3.98E-05	6.60E-04	0.21472±0.00334	4.50278±0.05472	0.30633±0.00317	0.8507	0.10661±0.00068	1720±18	1742±12	1.28
645-16.1	1	43	45	1.09	11	5.36E-04±8.69E-05	1.39E-03	0.34661±0.00646	4.47452±0.07579	0.31127±0.00337	0.6390	0.10426±0.00136	1753±19	1701±24	-3.07
645-17.1	1	101	81	0.82	27	2.25E-04±4.43E-05	6.20E-04	0.25414±0.00356	4.52157±0.05729	0.30794±0.00328	0.8417	0.10649±0.00073	1729±18	1740±13	0.63
645-19.1	1	80	44	0.57	21	2.83E-04±5.20E-05	1.02E-03	0.18262±0.00337	4.52206±0.05941	0.31047±0.00323	0.7930	0.10564±0.00085	1745±18	1725±15	-1.16
645-20.1	1	79	47	0.61	21	1.49E-04±4.98E-05	4.69E-04	0.19282±0.00352	4.56917±0.05942	0.30874±0.00325	0.8096	0.10733±0.00082	1732±18	1755±14	1.31
645-21.1	1	137	77	0.58	36	1.29E-04±3.32E-05	6.06E-04	0.17772±0.00256	4.52011±0.05219	0.30640±0.00314	0.8871	0.10699±0.00057	1720±17	1749±10	1.69
645-24.1	1	53	41	0.79	14	4.27E-04±7.78E-05	1.08E-03	0.25391±0.00494	4.55875±0.07171	0.31118±0.00337	0.6887	0.10625±0.00121	1748±19	1736±21	-0.69
645-25.1	1	76	55	0.75	20	3.41E-04±4.73E-05	3.70E-04	0.23411±0.00403	4.52352±0.07065	0.31007±0.00423	0.8724	0.10581±0.00081	1743±23	1728±14	-0.84
645-26.1	1	91	52	0.59	24	1.96E-04±4.66E-05	7.52E-04	0.18508±0.00318	4.52117±0.05698	0.30731±0.00319	0.8225	0.10670±0.00076	1725±18	1744±13	1.07
645-28.1	1	84	60	0.74	23	2.19E-04±7.46E-05	7.93E-04	0.22650±0.00372	4.59449±0.06814	0.31411±0.00328	0.7051	0.10608±0.00112	1764±18	1733±19	-1.83
645-30.1	1	65	39	0.61	17	3.78E-04±8.24E-05	1.22E-03	0.19749±0.00388	4.53410±0.07111	0.30732±0.00325	0.6735	0.10700±0.00124	1725±18	1749±21	1.40
645-36.1	3	55	42	0.79	15	2.23E-05±8.50E-06	5.07E-05	0.24087±0.00467	4.54986±0.05441	0.30926±0.00338	0.9139	0.10670±0.00052	1736±19	1744±9	0.44
645-38.1	3	133	73	0.56	35	-6.69E-06±-8.86E-06	-2.33E-05	0.17078±0.00252	4.51945±0.04925	0.30726±0.00320	0.9548	0.10668±0.00035	1725±18	1743±6	1.06
645-42.1	3	55	45	0.85	15	1.45E-04±3.70E-05	1.63E-04	0.24826±0.00482	4.54941±0.06853	0.31043±0.00417	0.8913	0.10629±0.00073	1744±23	1737±13	-0.40
645-48.1	3	69	53	0.79	18	5.41E-08±5.41E-06	7.84E-08	0.23439±0.00420	4.59213±0.05925	0.30960±0.00376	0.9416	0.10757±0.00047	1736±21	1759±8	1.30
645-50.1	3	98	49	0.51	26	5.38E-06±1.13E-05	1.61E-05	0.15211±0.00281	4.58606±0.05150	0.31099±0.00328	0.9389	0.10695±0.00041	1745±18	1748±7	0.17
645-51.1	3	42	26	0.64	11	7.36E-05±7.98E-05	9.62E-05	0.19210±0.00482	4.40841±0.07599	0.30072±0.00381	0.7356	0.10632±0.00124	1689±21	1737±21	2.77
645-56.1	3	65	61	0.97	17	4.87E-05±4.45E-05	1.20E-04	0.28540±0.00677	4.46273±0.05810	0.30577±0.00331	0.8312	0.10586±0.00077	1719±18	1729±13	0.62
645-57.1	3	84	58	0.71	22	-2.09E-06±-2.14E-06	-5.77E-06	0.21273±0.00357	4.54668±0.05142	0.30714±0.00327	0.9404	0.10736±0.00041	1723±18	1755±7	1.85

82LAA-T305-1, Quartz feldspar porphyry dyke
Notes (*see* Stern, 1997)
Spot name follows the convention x-y.z; where x = sample number, y = grain number and z = spot number. Multiple analyses in an individual spot are labelled as "x-y.z.z"
Uncertainties reported at 1s (absolute) and are calculated by numerical propagation of all known sources of error.
$f(206)_{204}$ refers to mole fraction of total ^{206}Pb that is due to common Pb, calculated using the ^{204}Pb-method; common Pb composition used is the surface blank (4/6: 0.05770; 7/6: 0.89500; 8/6: 2.13840)
* refers to radiogenic Pb (corrected for common Pb)
Discordance relative to origin = 100 * (($^{207}Pb/^{206}Pb$ age -$^{206}Pb/238U$ age)/($^{207}Pb/^{206}Pb$ age))
Error in $^{206}Pb/^{238}U$ calibration 1%
Th/U calibration: F = 0.03900*UO + 0.85600

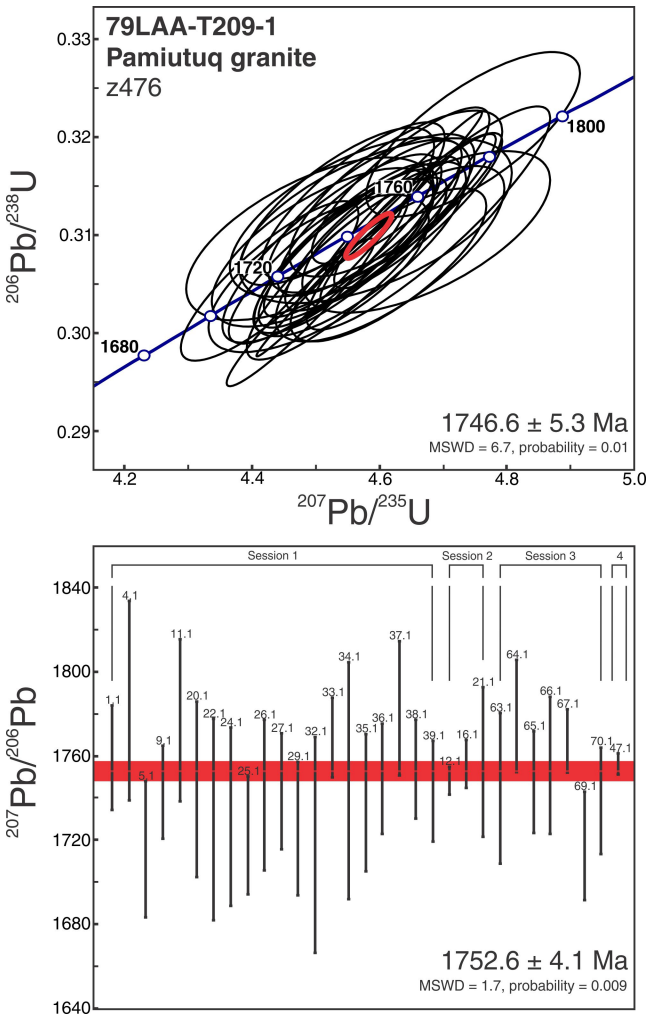

Figure 12. Concordia diagram and weighted average summary for Pamiutuq granite zircon.

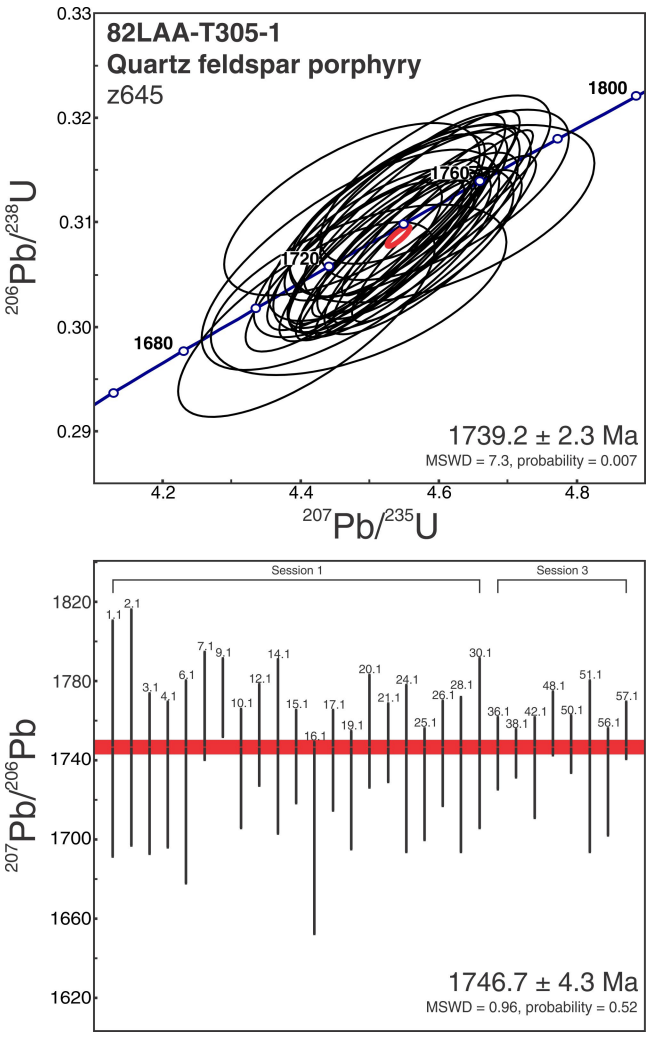

Figure 13. Concordia diagram and weighted average summary for quartz-feldspar porphyry dyke zircon.

The Mallery complex and epithermal mineralization

The crystallization age for baddeleyite of the Mallery gabbro (this study) is 1769 ± 6 Ma. An age for the granite in the centre of the Mallery complex determined by Turner et al. (2003) of 1755.4 ± 1.8 Ma is based on a regression of only three of their seven zircon analyses, and omits two fractions that plot to the right of that regression. The omitted fractions have $^{207}Pb/^{206}Pb$ ages of 1763 and 1761 Ma (2.4% and 0.8% discordant, respectively). Another regression was offered by these authors using all of the data, which gave an upper intercept age of 1759.9 ± 6.5 Ma (or 1760 ± 7 Ma). Therefore, a more accurate (if less precise) age for the granite may actually be closer to 1760 Ma than to 1755 Ma.

The Mallery granite age is significant, since the complex can be interpreted as a ring intrusion where the core granite and outer gabbro would be expected to be part of the same intrusive event and therefore close in age. A 14 Ma gap between the intrusions, as implied by the published U-Pb age of the granite, would require that the position of the granite is a coincidence (though perhaps, structurally controlled). If the older age for the granite is preferred, the midpoint of the error overlap of the gabbro and granite is at approximately 1765 Ma.

Biczok (1996) interpreted agate-fluorite mineralization in the map area as a late syn-volcanic phenomenon. Turner (2000) and Turner et al. (2001), in a study of fluid inclusions and stable isotopes, found this mineralization to be typical of Phanerozoic epithermal deposits associated with felsic volcanism. Quartz-rich epithermal zones are also common on the margins of Proterozoic rapakivi plutons in Finland (Haapala and Lukkari, 2005). We therefore consider that the approximately 1423 Ma fluorite Sm-Nd errorchron age obtained by Turner et al. (2003) reflects later resetting of the Sm-Nd system and is not the formation age of the mineralization which, as an epithermal phenomenon, should be

the same or slightly younger than the Pitz Formation and Nueltin granites. We are not aware of thermal or uplift events which might have caused widespread formation of high-temperature agates any time after approximately 1.75 Ga in this area. As it is not known where the LREEs reside in the fluorite (solid inclusions, fluid inclusions, or the crystal lattice), it is impossible to estimate what the closing temperature of the system is.

Basalts, the Fish intrusion, and Pb-Cu mineralization

The basalts to the northeast of the dyke-like extension of the Fish intrusion, contain ilmenite-apatite microxenoliths (including pseudomorphs after clinopyroxene) very similar to intercumulate grains in the Fish intrusion. Considering the congruity of the elemental and isotopic composition of these rocks, we conclude that the basalts, the Fish intrusion, and the Mallery gabbro had a similar source and are likely of a similar age.

The presence of the Spec Lake mineral occurrence north of the Fish intrusion and smaller Pb-Cu showings flanking its extrapolated extension to the northeast, indicates that Cu-Pb mineralization is perhaps related to this intrusion, rather than to a later, unexposed Nueltin granite intrusion (Webb, 1981). As noted above, the Spec Lake showing has a minimum Pb-Pb model age of 1.77 Ga, similar to the emplacement age of the Mallery gabbro.

Silicic rocks and the time span of Kivalliq activity

The observed correlation between mafic rock type and age raises the question of whether a secular variation in silicic magma types can also be identified. The age obtained here for the subvolcanic Pamiutuq intrusion (1752.6 ± 4.1 Ma) is older than the age of the quartz-feldspar porphyry dyke near the Fish intrusion (1746.7 ± 4.3 Ma), although the error ranges overlap. This is consistent with the field relations summarized by Booth (1983), who observed that numerous quartz-feldspar porphyry dykes, frequently rapakivi-textured or with 'proto-rapakivi' rounded alkali feldspar phenocrysts, cut the Pamiutuq intrusion. LeCheminant et al. (1981) concluded that the porphyry dykes were equivalent to rapakivi granite bodies north and west of the Pamiutuq intrusion, and that the rapakivi intrusions were broadly younger than most other Nueltin granites. However, the McRae Lake dyke (1753.6 ± 1.2 Ma) postdates one porphyry dyke and also cuts the Pitz Formation, which contains rhyolite lavas that are the extrusive equivalent of some Nueltin intrusions. We therefore are unable to conclusively identify any secular trend in Nueltin Granite composition or texture within this map area. More U-Pb ages, and particularly ones linked to the stratigraphy, are needed to better understand the progress of granite melt generation. At present, we can only conclude that granites/rhyolites were intruded/erupted throughout the entire time that mantle-derived basalt was being generated. A histogram of all available U-Pb ages indicates that the peak of this activity occurred near 1755 Ma (Peterson et al., 2015).

Currently, the youngest U-Pb age yet obtained for the Kivalliq Suite is 1740 ± 2 Ma, for a rhyolite at the site of the Chalcedony Stockwork epithermal showing in NTS 65-O (Turner, 2000). In a study of Cenozoic topaz rhyolites of the western U.S., Drew et al. (2013) concluded that glassy, sparsely porphyritic rhyolite lavas, which erupt near or above their liquidus temperature, can form by remelting of hydrothermally altered rhyolite deposited in an earlier phase of the volcanic cycle (and are highly unlikely to originate in the lower to middle crust as they would develop a phenocryst population during ascent). Such rhyolites are typically more aluminous than the norm, and are commonly topaz-bearing. Aphyric rhyolites are widespread within the Pitz Formation, where they occur in erosionally resistant domes (Peterson et al., 2015). An example is located near the east edge of 65-O (location "G," Fig. 1). None of the highly glassy or topaz-bearing rhyolites of the Kivalliq Suite has yet been dated. We speculate that these rocks will prove to be the youngest rhyolites and that the complete time range of Kivalliq activity will prove to exceed 30 million years. We also note that the glassy rhyolite domes are likely to overlie hydrothermally altered rocks and may, therefore, be indicators of related subsurface mineral deposits (e.g. Au-Ag, Sn).

We find that the apparent 30 million year span of Kivalliq Suite igneous activity extends beyond that previously determined by van Breemen et al. (2005), and is represented within this single map area. These results reinforce the conclusion of Peterson et al. (2015) that the Tebesjuak-Tulemalu area represents the central focus of Kivalliq activity, where volcanism first began and also persisted the longest. Much of the additional research required to understand this dramatic anorogenic event, which is expressed in outlying igneous centres and lower crustal metamorphic zircons from Somerset Island to southern Alberta (Peterson et al., 2015) could be conducted within this map area.

Future work

Our study — intended to clarify the age and nature of Kivalliq igneous activity in the map area — has revealed additional knowledge deficiencies, and raised additional questions. The following work is required to address these questions: 1) dating of the metasomatic zircons of the Mallery gabbro, and re-evaluation of the age of the core granite body; 2) U-Pb dating of the Fish intrusion and correlated basalts; 3) additional geochronological studies of silicic rocks and geochemical (e.g. stable isotope) studies of glassy/topaz rhyolites; and 4) detailed lithological and geochronological studies in arenaceous sequences on the margins of the Pitz Formation here assigned to the Amarook Formation.

ACKNOWLEDGMENTS

The first author thanks Daniel Bazor for field assistance in 2012. A review by B. Kjarsgaard improved the manuscript. The forward-looking leadership of C. Jefferson (GEM1-U) is strongly reflected in this work.

REFERENCES

Alviola, R., Johanson, B.S., Ramo, O.T., and Vaasjoki, M., 1999. The Proterozoic Ahvenisto rapakivi granite-massif-type anorthosite complex, southeastern Finland; petrography and U-Pb geochronology; Precambrian Research, v. 95, p. 89–107. doi:10.1016/S0301-9268(98)00128-4

Biczok, J., 1996. Mallery Lake Project, NWT: 1996 geological exploration report; Government of Canada, Department of Indian and Northern Affairs Report 083797.

Bonin, B., 1986. Ring complexes and anorogenic magmatism; North Oxford Academic Publishers Ltd, Oxford, United Kingdom; 189 p.

Booth, G.W., 1983 The petrology and geochemistry of the Pamiutuq Lake batholith, Northwest Territories; M.Sc. thesis, University of Toronto, Toronto, Ontario, 176 p.

Buchan, K.L. and Ernst, R.E., 2013. Diabase dyke swarms of Nunavut, Northwest Territories and Yukon, Canada; Geological Survey of Canada Open File 7464, 24 p. doi:10.4095/293149

Burton, J.D., 1981. A wollastonite occurrence within volcanic rocks in the Keewatin District, Northwest Territories; B.Sc. thesis, University of Ottawa, Ottawa, Ontario, 80 p.

Chamberlain, K.R., Schmitt, A.K., Swapp, S.M., Harrison, T.M., Swoboda-Colberg, N., Bleeker, W., Peterson, T.D., Jefferson, C.W., and Khudoley, A.K., 2010. In-situ U-Pb (IN_SIMS) micro-baddeleyite dating of mafic rocks: Method with examples; Precambrian Research, v. 183, p. 379–387. doi:10.1016/j.precamres.2010.05.004

Drew, D.L., Bindeman, I.N., Watts, K.E., Schmitt, A.K., Fu, B., and McCurry, M., 2013. Crustal-scale recycling in caldera complexes and rift zones along the Yellowstone hotspot track: O and Hf isotopic evidence in diverse zircons from voluminous rhyolites of the Picabo volcanic field, Idaho; Earth and Planetary Science Letters, v. 381, p. 63–77. doi:10.1016/j.epsl.2013.08.007

Fuchs, H.D. and Hilger, W., 1989. Kiggavik (Lone Gull): an unconformity related uranium deposit in the Thelon Basin, Northwest Territories, Canada. Uranium Resources and Geology of North American: Internation Atomic Energy Agency; Technical Document, v. 500, p. 429–454.

Haapala, I. and Lukkari, S., 2005. Petrological and geochemical evolution of the Kymi stock, a topaz granite cupola within the Wiborg rapakivi batholith, Finland; Lithos, v. 80, p. 347–362. doi:10.1016/j.lithos.2004.05.012

Haapala, I., Rämö, O.T., and Frindt, S., 2005. Comparison of Proterozoic and Phanerozoic rift-related basaltic-granitic magmatism; Lithos, v. 80, p. 1–32. doi:10.1016/j.lithos.2004.04.057

Jaffey, A.H., Flynn, K.F., Glendenin, L.E., Bentley, W.C., and Essling, A.M., 1971. Precision measurements of half-lives and specific activities of ^{235}U and ^{238}U; Physical Review C: Nuclear Physics, v. 4, p. 1889–1906. doi:10.1103/PhysRevC.4.1889

Jebrak, M., Marcoux, E., and Fontaine, D., 1996. Hydrothermal silica-gold stalactites formed by colloidal deposition in the Cirotan epithermal deposit, Indonesia; Canadian Mineralogist, v. 34, p. 931–938.

Jefferson, C., Pehrsson, S., Peterson, T., Chorlton, S., Davis, B., Keating, P., Gandhi, S., Fortin, R., Buckle, J., Miles, W., Rainbird, R., Lecheminant, T., Tschirhart, V., Tschirhart, P., Morris, W., Scott, J., Cousens, B., McEwan, B., Bethune, K., Riemer, W., Calhoun, L., White, J., MacIsaac, D., Leblon, B., Lentz, D., LaRocque, A., Shelat, Y., Patterson, J., Enright, A., Stieber, C., and Riegler, T., 2011a. Northeast Thelon region geoscience framework - new maps and data for uranium in Nunavut; Geological Survey of Canada Open File 6949, poster. doi:10.4095/288791

Jefferson, C.W., Chorlton, L.B., Pehrsson, S.J., Peterson, T.D., Wollenberg, P., Scott, J., Tschirhart, V., McEwan, B., Bethune, K., Calhoun, L., White, J.C., Leblon, B., LaRocque, A., Shelat, Y., Lentz, D., Patterson, J., Riegler, T., Skulski, T., Robinson, S., Paulen, R., McClenaghan, M.B., Layton-Matthews, D., MacIsaac, D., Riemer, W., Stieber, C., and Tschirhart, P., 2011b. Northeast Thelon Region: geomapping for uranium in Nunavut; Geological Survey of Canada Open File 6962, 38 p.

Jefferson, C.W., White, J.C., Young, G.M., Patterson, J., Tschirhart, V., Calhoun, L., Rainbird, R.H., Peterson, T., Davis, W.J., Tella, S., Chorlton, L.B., Scott, J.M.J., Davis, W.J., Morris, W.A., Anand, A., Shelat, Y., and MacIsaac, D., in press. Outcrop and remote predictive geology of the Amer Belt and basement beside and beneath the northeast Thelon Basin in parts of NTS 66A, B, C, F, G and H, Nunavut. Geological Survey of Canada Open File 7242, 1 sheet.

Krogh, T.E., 1973. A low contamination method for the hydrothermal decomposition of zircon and extraction of U and Pb for isotopic age determinations; Geochimica et Cosmochimica Acta, v. 37, p. 485–494. doi:10.1016/0016-7037(73)90213-5

LeCheminant, A.N., 1981. Geology, Tebesjuak Lake, District of Keewatin; Geological Survey of Canada Open File 728. doi:10.4095/129725

LeCheminant, A.N. and Heaman, L.M., 1989. Mackenzie igneous events, Canada: Middle Proterozoic hotspot magmatism associated with ocean opening; Earth and Planetary Science Letters, v. 96, p. 38–48. doi:10.1016/0012-821X(89)90122-2

LeCheminant, A.N., Lambert, M.B., Miller, A.R., and Booth, G.W., 1979a. Geological studies: Tebesjuak Lake map area, District of Keewatin: *in* Current Research Part A; Geological Survey of Canada Paper 79–1A, p. 179–186.

LeCheminant, A.N., Miller, A.R., Booth, G.W., Murray, M.J., and Jenner, G.A., 1979b. Geology of the Tebesjuak Lake map area: a progress report with notes on uranium and base metal mineralization; Geological Survey of Canada Open File 663, 26 p. doi:10.4095/129571

LeCheminant, A.N., Miller, A.R., Booth, G.W., Murray, M.J., and Jenner, G.A., 1980. Geology of the Tebesjuak Lake map area, District of Keewatin: a progress report with notes on uranium and base metal mineralization; *in* Current Research Part A; Geological Survey of Canada Paper 80–1A, p. 339–346.

LeCheminant, A.N., Ianelli, T.R., Zaitlin, B., and Miller, A.R., 1981. Geology of Tebesjuak Lake map area, District of Keewatin: a progress report: *in* Current Research Part B; Geological Survey of Canada Paper 81–1B, p. 113–128.

Ludwig, K.R., 2003. User's manual for Isoplot 3.00: a geochronological toolkit for Microsoft Excel; Berkeley Geochronology Center, Berkeley, California, 74 p.

Parrish, R.R., Roddick, J.C., Loveridge, W.D., and Sullivan, R.W., 1987. Uranium-lead analytical techniques at the Geochronology Laboratory, Geological Survey of Canada; *in* Radiogenic Age and Isotopic Studies, Report 1, Geological Survey of Canada Paper 87–2, p. 3–7.

Peterson, T.D., 2006. Geology of the Dubawnt Lake area, Nunavut-Northwest Territories; Geological Survey of Canada Bulletin 580, 56 p. doi:10.4095/221939

Peterson, T.D. and van Breemen, O., 1999. Review and progress report of Proterozoic granitoid rocks of the western Churchill Province, Northwest Territories (Nunavut); in Current Research 1999-C; Geological Survey of Canada , p. 119–127.

Peterson, T.D., Scott, J.M.J., LeCheminant, A.N., Chorlton, L.B., D'Aoust, B., 2014. Geology, Tebesjuak Lake area (NTS 65O). Geological Survey of Canada Canadian Geoscience Map 158, scale 1:250 000. doi:10.4095/293892

Peterson, T.D., Scott, J.M.J., LeCheminant, A.N., Jefferson, C.W., and Pehrsson, S.J., 2015. The Kivalliq Igneous Suite: Anorogenic bimodal magmatism at 1.75 Ga in the western Churchill Province, Canada; Precambrian Research, v. 262, p. 101–119. doi:10.1016/j.precamres.2015.02.019

Rainbird, R.H., Hadlari, T., Aspler, L.B., Donaldson, J.A., LeCheminant, A.N., and Peterson, T.D., 2003. Sequence stratigraphy and evolution of the Paleoproterozoic intracontinental Baker Lake and Thelon basins, western Churchill Province, Nunavut, Canada; Precambrian Research, v. 125, p. 21–53. doi:10.1016/S0301-9268(03)00076-7

Roberts, K.A., 1981. Geology of the Dick Lake contact aureole; B.Sc. thesis, Carleton University, Ottawa, Ontario, 51 p.

Roddick, J.C., 1987. Generalized numerical error analysis with applications to geochronology and thermodynamics; Geochimica et Cosmochimica Acta, v. 51, p. 2129–2135. doi:10.1016/0016-7037(87)90261-4

Scott, J.M., 2012. Petrology, lithogeochemistry and geochronology of Nueltin Suite associated with uranium mineralization in the Northeast Thelon region, Nunavut. M.Sc. thesis, Carleton University, Ottawa, Ontario, 141 p.

Scott, J.M., Peterson, T.D., Davis, W.J., Jefferson, C.W., and Cousens, B.L., in press: Petrology and geochronology of Paleoproterozoic intrusive rocks, Kiggavik uranium camp, Nunavut; Canadian Journal of Earth Sciences. doi:10.1139/cjes-2014-0153

Stacey, J.S. and Kramers, J., 1975. Approximation of terrestrial lead isotope evolution by a two-stage model; Earth and Planetary Science Letters, v. 26, p. 207–221. doi:10.1016/0012-821X(75)90088-6

Stern, R.A., 1997. The GSC Sensitive High Resolution Ion Microprobe (SHRIMP); analytical techniques of zircon U–Th–Pb age determinations and performance evaluation; *in* Radiogenic Age and Isotopic Studies: Report 10; Geological Survey of Canada Current Research 1998-F, p. 1–31.

Stern, R.A. and Amelin, Y., 2003. Assessment of errors in SIMS zircon U–Pb geochronolgoy using a natural zircon standard and NIST SRM 610 glass; Chemical Geology, v. 197, p. 111–142. doi:10.1016/S0009-2541(02)00320-0

Tambosso, A.W., 1981. Geology of the McRae Lake Dyke, District of Keewatin, Northwest Territories. B.Sc. thesis, University of Toronto, Toronto, Ontario, 145 p.

Tschirhart, V., Morris, W.A., and Oneschuk, D., 2011. Geophysical series, geophysical compilation project, Thelon Basin, Nunavut, NTS 66A, B, and parts of 65N, O, P, 66C, F, G and H; Geological Survey of Canada, Open File 6944. doi:10.4095/288806

Turner, W.A., 2000. Geology and Geochemistry of the Mallery Lake precious metal-bearing epithermal system, Nunavut, Canada. Ph.D. thesis, Department of Earth and Atmospheric Sciences, University of Alberta, Edmonton, Alberta, 186 p.

Turner, W.A., Richards, J.P., Nesbitt, B.E., Muehlrnbachs, K., and Biczok, J.L., 2001. Proterozoic low-sulfidation epithermal Au-Ag mineralization in the Mallery Lake area, Nunavut, Canada; Mineralium Deposita, v. 36, p. 442–457. doi:10.1007/s001260100181

Turner, W.A., Heaman, L.M., and Creaser, R.A., 2003. Sm-Nd fluorite dating of Proterozoic low-sulfidation epithermal Au-Ag deposits and U-Pb zircon dating of host rocks at Mallery Lake, Nunavut, Canada; Canadian Journal of Earth Sciences, v. 40, p. 1789–1804. doi:10.1139/e03-061

van Breemen, O., Peterson, T.D., and Sandeman, H.A., 2005. U-Pb zircon geochronology and Nd isotope geochemistry of Proterozoic granitoids in the western Churchill Province: intrusive age pattern and Archean source domains; Canadian Journal of Earth Sciences, v. 42, p. 339–377. doi:10.1139/e05-007

Webb, D.R., 1981. A lead, copper vein occurrence at Spec Lake, District of Keewatin, Northwest Territories. B.Sc. thesis, University of Toronto, Toronto, Ontario, 98 p.

Geological Survey of Canada Project 340521NU62